REPORT DOCUMENTATION PAGE

AFOSR-TR-96 97 0127

1. AGENCY USE ONLY (Leave blank)	2. REPORT DATE	3. REPORT TYPE AND DATES COVERED
	Dec. 30, 1996	Final Report

4. TITLE AND SUBTITLE
Luminescent Paint for Pressure and Temperature Measurements on Rotating Machinery

5. FUNDING NUMBERS
AFOSR Grant Number F49620-95-1-0031

6. AUTHOR(S)
John Sullivan, Tianshu Liu, Steve Burns, and Bryan Campbell

7. PERFORMING ORGANIZATION NAME(S) AND ADDRESS(ES)
Purdue University
School of Aeronautics and Astronautics
Grissom Hall 1282
West Lafayette, IN 47907-1282

8. PERFORMING ORGANIZATION REPORT NUMBER

9. SPONSORING/MONITORING AGENCY NAME(S) AND ADDRESS(ES)
AFOSR/NA
110 Duncan Avenue, Suite B115
Bolling AFB, DC 20332-0001

NA

10. SPONSORING/MONITORING AGENCY REPORT NUMBER
95-1-0031

11. SUPPLEMENTARY NOTES

12a. DISTRIBUTION/AVAILABILITY STATEMENT
unlimited

12b. DISTRIBUTION CODE

13. ABSTRACT *(Maximum 200 words)*

This report is an overview of the current state of temperature- and pressure-sensitive luminescent paint techniques. Topics include photophysical foundations, paint preparation and calibration, measurement systems, accuracy, and time response. Applications of the luminescent paint technique in aerodynamic testing are discussed and results of measurements of a transonic rotor are presented.

14. SUBJECT TERMS	15. NUMBER OF PAGES
pressure paint, temperature paint, transonic compressor	93
	16. PRICE CODE

17. SECURITY CLASSIFICATION OF REPORT	18. SECURITY CLASSIFICATION OF THIS PAGE	19. SECURITY CLASSIFICATION OF ABSTRACT	20. LIMITATION OF ABSTRACT

Luminescent Paint for Pressure and Temperature Measurements on Rotating Machinery

Principal Investigator Professor John Sullivan
Graduate Students - Tianshu Liu, Steve Burns, Bryan Campbell
Purdue University
School of Aeronautics and Astronautics

ABSTRACT

This paper presents an overview of the current state of temperature- and pressure-sensitive luminescent paint techniques. Topics include photophysical foundations, paint preparation and calibration, measurement systems, accuracy, and time response. Applications of the luminescent paint technique in aerodynamic testing are discussed and typical examples of current research are given.

1. INTRODUCTION

In recent years, new techniques based on luminescence quenching have been developed for measuring temperature and pressure distributions on wind tunnel models. These new sensors are called temperature-sensitive paint (TSP) and pressure-sensitive paint (PSP). Traditionally, arrays of thermocouples and pressure taps have been used to obtain surface temperature and pressure distributions. These techniques can be very labor-intensive and model preparation costs are high when detailed maps of temperature

and pressure are desired. Further, spatial resolution is limited by the number of instrumentation locations chosen. By comparison, the TSP and PSP techniques provide a way to obtain simple, inexpensive, full-field measurements of temperature and pressure with much higher spatial resolution. Both TSPs and PSPs incorporate luminescent molecules in a paint which can be applied to any aerodynamic model surface. Figure 1 shows a schematic of a paint layer incorporating a luminescent molecule.

The paint layer is composed of luminescent molecules and a polymer binder material, both of which can be dissolved in a solvent. The resulting 'paint' can be applied to a surface using a brush or sprayer. An alternative method of applying the paint is to deposit the polymer matrix on the surface first and then apply the luminophore in solvent solution to the polymer layer. As the paint dries, the solvent evaporates and leaves behind a polymer matrix with luminescent molecules embedded in it. Light of the proper wavelength to excite the luminescent molecules in the paint is directed at the model and luminescent light of a longer wavelength is emitted by the molecules. Using the proper filters, the excitation light and luminescent emission light can be separated and the intensity of the luminescent light can be determined using a photodetector. Through the photo-physical processes known as thermal- and oxygen-quenching, the luminescent intensity of the paint emission can be related to temperature or pressure. Hence, from the detected luminescent intensity, temperature or pressure can be determined. A detailed discussion of the foundations of the luminescent paint technique will be presented later.

1.2 History of temperature-sensitive paints

An europium-based TSP system in a polymer binder was developed by Kolodner et al. (1982, 1983a, 1983b) at Bell Laboratory to measure the surface temperature distribution of an operating integrated circuit. This paint system was adapted at Purdue University for aerodynamic testing (Campbell et al. 1992, 1993, 1994, Liu et al. 1992, 1994a, 1994b, 1995a, 1995b, 1996a, 1996b). TSP formulations were also studied by a group of chemists at the University of Washington (Gallery 1993) and one of their paints has been used for transition detection at NASA-Ames (McLachlan et al. 1993b). A similar method for measuring surface temperature distributions utilizes microcrystalline thermographic phosphors. This technique has the same photophysical foundations as the TSP method. However, unlike the polymer-based TSP system, thermographic phosphors are usually applied to a model surface in powder or crystal form. Thermographic phosphors have been used in fiber-optic thermometry systems for testing of electronics systems (Wickersheim and Sun 1985). Aerodynamic applications of thermographic phosphors mixed with binders and ceramic materials were first explored by Bradley (1953) to measure surface temperature and further used in high speed wind tunnels by Czysz and Dixon (1969) at McDonnell Douglas and Buck (1988, 1989, 1991) at NASA-Langley. Thermographic phosphors for temperature measurement in gas turbine engines were developed by Noel et al. (1985, 1986, 1987), Tobin et al. (1990), and Alaruri et al. (1995). Other methods used to obtain surface temperature maps are liquid crystals (Hippensteele et al. 1983, 1985, Babinsky and Edwards 1993) and infrared thermography (Gartenburg and Robert 1991). Generally speaking, these two-dimensional techniques all provide surface temperature distributions at higher resolution than thermocouples. Some

are more sensitive, some have faster time response, and some have a broader range of temperature measurement.

1.3 History of pressure-sensitive paints

In 1980, Peterson and Fitzgerald demonstrated a surface flow visualization technique based on oxygen quenching of dye fluorescence. Their preliminary experiment revealed the possibility of using the oxygen-quenching sensor for surface pressure measurement. The Central Aero-Hydrodynamic Institute (TsAGI) in Russia was one of the pioneers of the PSP technique for aerodynamic testing, and jointly developed a PSP system with the Italian firm INTECO (Ardasheva et al. 1985, Volan and Alati 1991, Bukov et al. 1992, Bukov et al. 1993, Troyanovsky et al. 1993). INTECO's system was demonstrated in several wind tunnel tests in the early 1990s in the United States and Germany. Pressure sensitive paints were developed independently in the United States by a group based at the University of Washington (Gouterman et al. 1990, Kavandi et al. 1990). Their early paints used platinum-octaethylporphorin (PtOEP) as the luminescent molecule, and newer work has concentrated on several proprietary paint formulations. Considerable work on the PSP technique has also been done at McDonnell Douglas (Morris et al. 1993a, 1993b, 1995, Donovan et al. 1993, Dowgwillo, et al. 1994, Crites 1993), NASA-Ames (McLachlan et al. 1993a, 1993b, 1995a, 1995b, Bell and McLachlan 1993) and Boeing. European researchers have also been working on PSP systems (Engler et al. 1991a, 1991b, Engler 1995, Davies et al. 1995). More and more institutions are becoming interested in developing the PSP technique because of its high spatial resolution and low cost.

2. PHOTOPHYSICAL FOUNDATIONS

This section provides a brief description of the luminescence and quenching processes which lay the photophysical foundation for the TSP and PSP techniques. More detailed discussions of the mechanisms underlying photophysical processes in polymers and solutions are given by Rabek (1987), Becker (1969), and Parker (1968). Molecular photoluminescence (fluorescence and phosphorescence) is a radiative phenomenon that occurs when a molecule absorbs a photon of light. When one of a pair of electrons in a molecule is excited to a higher energy level, there are two permitted states: the singlet state (S_i) and the triplet state (T_i). In the singlet state, the spin of the promoted electron is paired with the ground state electron. In the triplet state, however, the spins of the two electrons become unpaired. The excited singlet state is more energetic than the corresponding excited triplet state. More importantly, a singlet/singlet transition is much more probable than a singlet/triplet transition which involves a change in electronic state. As a consequence, direct excitation of a ground state molecule to the triplet state has a very low probability of occurrence. Therefore, after absorption of the photon, a molecule that is initially in the singlet ground state S_0 usually converts to the excited singlet state S_i ($i \geq 1$). Within picoseconds, the excited states S_i ($i > 1$) relax to the lowest singlet state S_1 through internal conversion without emission of radiation. The excitation energy in the S_1 state may be dissipated by emission of radiation or through radiationless deactivation. Fluorescence is the emission process produced by a transition from the S_1 to S_0 state. However, it is also possible for an excited molecule in the S_1 state to convert to an excited

triplet state by a radiationless transition called intersystem crossing. The lowest excited triplet state T_1 is formed by vibrational relaxation. Phosphorescence is the emission process produced by a transition from the T_1 to S_0 states. In contrast to fluorescence, phosphorescence is a delayed emission, typically with a longer lifetime. From an application standpoint, the most interesting fact is that the excited singlet and triplet states can be deactivated by quenching processes. Two important quenching processes are thermal quenching and oxygen quenching, which are related to the TSP and PSP techniques, respectively.

In order to quantify these photophysical processes, the quantum yield (or quantum efficiency) of luminescence Φ is introduced

$$\Phi = \frac{\text{rate of luminescence emission}}{\text{rate of excitation}} = \frac{I}{I_a} \tag{1}$$

where I is the luminescence intensity and I_a is the absorption intensity. The absorption intensity I_a can be described by the Beer-Lambert law

$$I_a = I_{ex}\,(1 - 10^{-\varepsilon c l_p}) \tag{2}$$

where ε is the molar absorptivity, c is the concentration of the absorbing species, l_p is the path length traversed by the light beam, and I_{ex} is the monochromatic excitation light intensity.

2.1 PSPs

For a PSP, the quantum yield of emission in the presence of an oxygen quencher is given by a simple model

$$\Phi = \frac{I}{I_a} = \frac{k_L}{k_L + k_D + k_Q[O_2]} = k_L \tau \qquad (3)$$

where k_L is the rate constant for luminescence emission, k_D is the rate constant for radiationless deactivation, k_Q is the rate constant for oxygen quenching, $[O_2]$ is the concentration of oxygen, and τ is the lifetime of an excited molecule. Dividing (3) into the quantum yield in the absence of oxygen i.e. $\Phi_0 = I_0 / I_a = k_L / (k_L + k_D)$, one can obtain the Stern-Volmer equation

$$\frac{I_0}{I} = 1 + k_Q \tau_0 [O_2] \qquad (4)$$

where I_0 and $\tau_0 = 1/(k_L + k_D)$ are the luminescent intensity and lifetime of an excited molecule in the absence of oxygen quencher, respectively. According to Henry's law, $[O_2] \propto P_{O_2}$ and further $[O_2] \propto P$, where P_{O_2} is the partial pressure of O_2 and P is the air pressure. By taking the ratio between I and a reference intensity I_{ref} at a known constant reference pressure P_{ref}, the Stern-Volmer relation can be put in a form suitable for aerodynamic testing purposes,

$$\frac{I_{ref}}{I} = A_0(T) + A_1(T)\frac{P}{P_{ref}} \qquad (5)$$

A more general expression is obtained by taking into account non-linear effects

$$\frac{I_{ref}}{I} = \sum_{n=0}^{N} A_n(T)\left(\frac{P}{P_{ref}}\right)^n . \qquad (6)$$

The coefficients A_n have to be determined through calibration tests. In practice, a second-order polynomial (N = 2) is adequate to give an accurate fit to experimental calibration data. Note that the absorption intensity I_a has been eliminated in (5) and (6). Therefore, the effects of spatial non-uniformities of illumination, paint thickness, and luminophore concentration can be eliminated by taking the ratio I/I_{ref}. This greatly simplifies the practical application of the PSP technique. Either (5) or (6) can serve as an operational calibration relation for a PSP in aerodynamic testing.

Note that the coefficients A_n are temperature-dependent since both the radiationless deactivation rate k_D and the oxygen diffusion and solubility in a polymer depend on temperature. The deactivation term k_D may be decomposed into a temperature-independent part k_0 and a temperature-dependent part k_1 that is related to thermally activated intersystem crossing (i.e. $k_D = k_0 + k_1$). The rate k_1 can be assumed to have an Arrhenius form (Bennett and McCartin 1966, Song and Fayer 1991)

$$k_1 = C\exp(-E/RT) \qquad (7)$$

where C is a constant, E is the Arrhenius activation energy, R is the universal gas constant and T is the thermodynamic temperature (in Kelvin). In addition to the intrinsic temperature dependence of the radiationless process, temperature can also affect gas diffusion in the polymer and thus influence oxygen quenching. For a diffusion-limited quenching reaction, the quenching rate constant k_Q can be described by the Smoluchowski equation (Szmacinski and Lakowicz 1995)

$$k_Q = 4\pi N p (D_P + D_Q) \tag{8}$$

where D_P and D_Q are the diffusion coefficients of the probe and quencher in the polymer, N is the number of molecules per millimole and p is a factor that depends on the quenching mechanism. Over small temperature ranges, the diffusion coefficients are related to temperature in the Arrhenius form. For example,

$$D_Q \propto \exp(-E_Q / RT) \tag{9}$$

where E_Q is the activation energy for the diffusion process of the quencher [O_2]. Which of these two mechanisms dominates temperature dependence of a PSP depends on the probe molecule and polymer binder used. Results obtained by Gewehr and Delpy (1993) show that the temperature dependence of oxygen diffusivity in a membrane of

polymethylmethacrylate (PMMA) has a stronger influence on the temperature dependence of luminescence for a Pd coproporphyrin probe.

2.2 TSPs

For a TSP, it is assumed that the paint layer is not oxygen-permeable so that $[O_2] = 0$. Hence, the quantum yield is simply given by

$$\Phi = \frac{I}{I_a} = \frac{k_L}{k_L + k_D} = k_L \tau_0 \qquad (10)$$

Relation (10) can be re-written by considering the temperature dependence (7) of the radiationless deactivation rate

$$\frac{I_a}{I(T)} - \frac{I_a}{I(0)} = A\, k_L^{-1} \exp(-E/RT) \qquad (11)$$

where I(0) is the luminescence intensity at absolute zero (T = 0). By dividing (11) by a reference intensity I_{ref} at a known constant temperature T_{ref}, the absorption intensity I_a can be eliminated. Hence, one has

$$\ln\left(\frac{I(T)\,[I(0) - I(T_{ref})]}{I(T_{ref})\,[I(0) - I(T)]}\right) = \frac{E}{R}\left(\frac{1}{T} - \frac{1}{T_{ref}}\right) \qquad (12)$$

In a normal working temperature range in which T is close to T_{ref}, the factor $[I(0) - I(T_{ref})] / [I(0) - I(T)]$ is nearly one. Hence, relation (12) can be approximately written in the simple Arrhenius form

$$\ln\left(\frac{I(T)}{I(T_{ref})}\right) = \frac{E}{R}\left(\frac{1}{T} - \frac{1}{T_{ref}}\right) \qquad (13)$$

Theoretically speaking, the Arrhenius plot of $\ln[I(T)/I(T_{ref})]$ versus $1/T$ gives a straight line of slope E/R. Tests indicate that the simple Arrhenius relation does fit experimental data over a certain temperature range. However, for some paints, the data may not fully obey the simple Arrhenius relation over a wider range of temperature. As an alternative, the relation between the luminescence intensity and temperature can be expressed in a functional form

$$\frac{I(T)}{I(T_{ref})} = F(T / T_{ref}) \qquad (14)$$

The empirical expression $F(T/T_{ref})$ could be a polynomial, exponential or other function which fits the experimental data over a certain temperature range. Both (13) and (14) are operational forms of the calibration relation for a TSP used for data reduction in practical applications.

3. PAINT FORMULATION

In general, both TSPs and PSPs are prepared by dissolving a luminescent substance in a polymer solution. Then, the mixtures can be applied on a surface by spraying, brushing or dipping. After the solvent evaporates, a thin smooth uniform film of the paint remains on the surface, in which the luminescent molecules are distributed in a polymer matrix. The polymer binder is an important ingredient of a luminescent paint and serves to adhere the paint to the surface of interest. In some cases, the polymer matrix is a passive anchor. In other cases, however, the polymer may significantly affect the photophysical behavior of the paint through a complicated interaction between the luminescent molecules and the macro-molecules of the polymer. Since the detailed role of the polymer support in controlling the photophysical processes is not well understood, it is basically a trial and error process to find an optimal combination of a luminophore and a polymer. A good polymer binder should be robust enough to sustain skin friction and other forces on the surface of an aerodynamic model. Also, it must be easily applied to the surface to get a thin smooth film (r.m.s. surface roughness is typically less than 1 μm). For TSPs, many commercially available resins and epoxies can serve as polymer binders if they are not oxygen permeable and do not degrade the activity of the luminophore molecules. In contrast, a good polymer binder for a PSP must have high oxygen permeability besides being robust and easy to apply.

3.1 TSPs

Table I lists many TSP formulations as well as their spectroscopic properties, temperature sensitivities and useful temperature measurement ranges. Data are collected from the theses of Campbell (1993), Gallery (1993), Bugos (1989) as well as other

sources. For comparison among different TSP formulations, the maximum logarithmic slope ($\max\{d[\ln(I / I_{ref})] / dT\}$) is used as an indicator of the temperature sensitivity of a TSP over a certain temperature range, where I_{ref} is a reference luminescence intensity. The logarithmic slope is used since it is independent of the reference intensity. Several proprietary temperature-sensitive paints are also included in Table I for comparison, although their formulations are not known. Many TSP coatings are temperature-sensitive over a range from -20 ^{0}C to 100 ^{0}C. Some can be used in a cryogenic temperature range from -180 ^{0}C to -50 ^{0}C. Most of the microcrystalline thermographic phosphors are suitable for high temperature measurements between 200 ^{0}C and 1100 ^{0}C.

Some TSP formulations have been successfully used to measure temperature in various applications. In their measurements of the surface temperature on an operating integrated circuit chip, Kolodner and Tyson (1982, 1983a, 1983b) used europium thenoyltrifluoroacetonate (EuTTA) doped into perdeutero-poly (methylmethacrylate) (dPMMA). A similar paint, EuTTA dissolved in model airplane dope (Aero Gloss, Pactra Inc.), has been applied to surface heat transfer measurements on aerodynamic models in supersonic and hypersonic flows (Liu et al. 1995a, 1995b) and boundary layer transition detection (Campbell 1993, Campbell et al. 1994). The paint made by mixing bipyridine ruthenous dichloride hexahydrate (Ru(bpy)) in Shellac (Clear Shellac, Zinsser Inc.) was used to demonstrate the feasibility of temperature measurement using a scanning laser system (Hamner et al. 1994) and a phase detection system (Campbell et al. 1994). Rhodamine B in polyurethane was developed for time-resolved thermal microscopy by Romano et al. (1989). Some TSPs for cryogenic temperature measurement have been

used for transition detection, including Ru(trpy)-GP197 and Ru(VH127)-GP197 (Campbell et al. 1994, Asai et al. 1996). High temperature thermographic phosphors have been used for turbine blade temperature measurement (Noel et al. 1985, 1986, 1987, Tobin et al. 1990, Alaruri et al. 1995). Detailed discussions on applications of TSP systems will be given later.

3.2 PSPs

Many PSP formulations are listed in Table II along with their spectroscopic properties and Stern-Volmer constants. In Table II, the Stern-Volmer constants A_0 and A_1 are the coefficients in the relation $I_{ref}/I = A_0 + A_1(P/P_{ref})$, where the reference pressure P_{ref} is ambient pressure (1 atm). For PSPs which do not completely obey the linear Stern-Volmer relation, the constants A_0 and A_1 are obtained by fitting data in a linear range. Results are collected from the theses of Wan (1993) and Burns (1995) and other sources, which documented the absorption spectra, emission spectra and Stern-Volmer plots of many oxygen sensing luminophores and supporting matrices. Table II also includes some formulations that were used as oxygen sensors in medical applications and are potentially useful in aerodynamic testing. Several proprietary PSP coatings have been successfully employed to measure surface pressure on aerodynamic models at TsAGI (Troyanovsky et al. 1993, Bukov et al. 1993), McDonnell Douglas (Morris et al. 1993a, 1993b, 1995) and NASA Ames (McLachlan and Bell 1995a). The Stern-Volmer constant A_1 of these proprietary PSP formulations is larger than 0.5, which generally indicates high pressure sensitivity (Oglesby et al. 1995a).

A well-known PSP used in aerodynamic testing is prepared by dissolving platinum octaethylporphyrin (PtOEP) in GP-197 resin solution (Kavandi et al. 1990, McLachlan et al. 1993a, 1995b). Some fast-response coatings were suggested by Baron et al. (1993). They are based on thin porous silica plates to which free-base tetra(pentafluorophenyl) porphyrin (H_2TFPP) dissolved in toluene is applied. Different porous silica plates include silica coating applied on an aluminum plate painted white (SILICA-W), silica coating applied to a bare aluminum plate (SILICA-B) and a commercial porous silica thin-layer chromatography plate (TLC). However, these fast-response coatings have not been used in wind tunnel tests. Perylene dye (Greengold) on a TLC plate was recently used on a rotating propeller blade to measure the surface pressure distribution (Burns and Sullivan 1995). Ru(bpy) absorbed onto a porous silica plate was used to measure the pressure distribution of an impinging air jet with a laser scanning system (Hamner et al. 1994).

For a PSP, the physical properties of the polymer binder are very important in determining pressure sensitivity and time response of the paint. The diffusivity of oxygen in the polymer is directly related to the time response of the paint. The solubility affects the penetration of oxygen into the polymer film and the amount of oxygen sorbed in the film under a certain pressure. The permeability, solubility and diffusion coefficients of many polymers and porous materials have been listed by Krevelen (1976), Mulder (1991), Fried (1995), and Robinson and Perlmutter (1994). Silica gel TLC plate is a highly porous binder for a luminophore. However, it is not robust enough to sustain abrasion and high friction and is very sensitive to moisture. These shortcomings limit its applications in aerodynamic testing. Silicone rubbers (e.g. RTV), which are highly permeable to oxygen

and very robust, have also been used as PSP binders. Other suitable polymers for PSPs can be found in the literature (Wan 1993, Gallery 1993, Xu et al. 1994). A sol-gel-derived coating that was used to provide a support matrix for an oxygen sensor may also be useful for PSPs (MacCraith et al. 1995).

In general, the behavior of a PSP depends on interactions between the polymer structure and the probe molecules. For instance, the non-linearity of the Stern-Volmer plot for a Ru(bpy)-silica-gel system results from microheterogeneity and Langmuir adsorption effects in the polymer matrix (Hartmann et al. 1995). Here, the microheterogeneity features very different environments provided by a solid-state matrix like the polymer for the probe molecule. The micro-environment of sensor molecules affects luminescence and quenching behavior. Meier et al (1995) found that the quenching efficiency can be much improved when the oxygen sensor (Ru(bpy) complex) is encapsulated in the cavities of a zeolite rather than absorbed onto the surface of either the zeolite or silica gel. Xu et al. (1994) reported that the oxygen quenching performance can be improved by adding a heterogeneous component, such as silica filler, into a pure homogeneous polymer. They also suggested guidelines for the design of suitable polymer supports for oxygen sensors. In addition, the polymer can be affected by temperature which in turn affects the performance of a PSP. Temperature can affect the coefficients of oxygen solubility, diffusivity and permeability of the polymer and thus change the pressure sensitivity and time response of a PSP. Hence, the Stern-Volmer coefficients depend on temperature not only due to changes in the rate of intersystem crossing, but also due to variations in the oxygen diffusivity that determines the bimolecular quenching rate.

Evidence for these phenomena is given in the experiments of Gewehr and Delpy (1993) who measured the temperature dependence of lifetime of a Pd coproporphyrin sensor in nitrogen and air. Finally, the choice of the polymer for a PSP should be based on overall considerations of its oxygen permeability, temperature effect, humidity effect, adhesion, mechanical stability, photodegradation and other characteristics.

4. CALIBRATION

Calibration tests must be made to characterize TSPs and PSPs before they can be used for aerodynamic testing. The calibration procedures for TSPs and PSPs are discussed in this section.

4.1 TSP calibration

In order to quantitatively measure temperature with the TSP coatings, a calibration relating luminescent intensity to temperature is needed. Figure 2 shows a schematic of a simple experimental set-up used for calibration of TSPs. The paint film is applied to an aluminum block (1.5 cm × 1.5 cm × 0.625 cm) which is thermally anchored using a high thermal conductivity grease to a Peltier heater/cooler which controls the temperature of the block. The temperature of the block is obtained from a thermometer probe placed in a hole near the painted surface. The paint is excited with an illumination source (typically a UV lamp or a laser) and the luminescent emission is focused through a lens and long-pass filter onto a photodetector (photodiode, PMT or CCD camera). The signal from the photodetector is amplified and fed to a PC computer. The dark current is subtracted from the intensity. The temperature data from the thermometer is also collected by the

computer. Hence, a calibration relation between the luminescence intensity and temperature can be obtained. The simple system in Fig. 2 has been adapted by Campbell et al. (1994) for calibration down to cryogenic temperatures. The paint sample is thermally anchored to a copper bar cut at an angle of 45° at its top which rests in a container filled with liquid nitrogen. Sample temperature near the temperature of liquid nitrogen can be achieved by heat conduction through the copper bar. In this case, care must be taken to prevent condensation of moisture from forming on the paint sample. This is accomplished using an airtight container for the sample which can be purged with dry nitrogen gas. The temperature-dependence of luminescent intensity for many paints has been examined using the above system (Campbell et al. 1994). Crovini and Fernicola (1992) designed a special oven for a fluorescent-decay temperature sensor in order to provide a controlled environment where temperature, pressure, and gas composition can be modified. In their set-up, the oven temperature stability is ± 0.03 °C and the temperature uniformity is ± 0.03 °C over the temperature range -20 to 200 °C.

Typical temperature dependencies of luminescent intensity are shown in Fig. 3 for some TSPs. Several TSPs have high temperature sensitivity in the cryogenic temperature range. Others can be used over a temperature range from -20 to 100 °C. Figure 4 shows the Arrhenius plots for EuTTA-dope and Ru(bpy)-Shellac paints. Data are obtained in calibration tests repeated over several days. The calibration curves are nearly linear over a certain temperature range on the Arrhenius plot.

4.2 PSP calibration

The set-up for PSP calibration is similar to that for TSPs, as shown Fig. 5. A PSP sample is placed inside a vacuum chamber with an optical access window. The pressure inside the chamber can be controlled and is measured using a pressure transducer. The temperature of the paint sample is controlled by a Peltier heater/cooler and monitored by a thermometer. Illumination light passes into the chamber and excites the luminescent paint. The luminescence emission is collected with a lens, filtered by a long-pass or band-pass optical filter and focused onto a photodetector. The photodetector signal is sampled by a PC computer at different pressures. Thus, the relation between luminescence intensity and pressure can be obtained at a constant temperature. The calibration data can be fit to the Stern-Volmer equation (5) or (6). Figure 6 shows the Stern-Volmer curves for several PSP formulations at ambient temperature (about 20 ^{0}C). When the calibration tests are carried out over a range of temperatures, the temperature dependence of the coefficients in the Stern-Volmer relation can be determined. Figure 7 show the Stern-Volmer plots for Ru(ph_2-phen) in GE RTV 118 at different temperatures. Both the slope and intercept of the Stern-Volmer plot tend to increase with temperature.

In practice, instead of a priori laboratory calibrations, some researchers opt to use in-situ pressure calibration to reduce some systematic errors in aerodynamic testing (Dowgwillo et al. 1994). In-situ calibration is performed on a model with pressure taps during a wind tunnel test by correlating the local pressure data obtained from the taps with the luminescent intensity at corresponding locations. In-situ calibration assumes that the model is iso-thermal such that the effects of temperature are eliminated. When the surface temperature distribution is not spatially uniform, the in-situ method fails. Recently, Engler

(1995) performed pixel-by-pixel calibration in the DLR transonic wind tunnel that can be continuously pressurized. Since the positions of the camera and illumination source are identical in calibrations and experiments, this method significantly improves the accuracy of PSP measurements. However, pixel-by-pixel calibration cannot be done in most wind tunnels since continuous pressurization is not available.

4.3 Lifetime (phase) calibration

The aforementioned calibrations are based on the measurement of the luminescent intensity as a function of temperature and pressure. As shown in section 2, the luminescent lifetime τ is also a function of temperature and pressure. In the lifetime (phase) detection system, a relation between the lifetime (phase) and temperature or pressure must be determined. The apparatus used for the luminescent intensity calibration in Figs. 2 and 5 can be adapted for lifetime calibration if the continuous excitation light source is replaced by a pulsed excitation light such as a pulsed laser or a flash lamp. After an exciting pulse has ceased, the exponential decay of the luminescence is measured by a photodetector and recorded with a PC computer or an oscilloscope. The luminescent lifetime can be determined at different temperatures and pressures by fitting the data with a simple exponential function $I(t) = I(0)\exp(-t/\tau)$. In some cases, a multi-exponential function is used to fit the experimental data. Early instruments used to measure lifetime were described by Brody (1957) and Bennett (1960). At present, lifetime measurement is a routine test in a photochemistry laboratory. Another method equivalent to direct lifetime measurement is phase detection. Due to the finite decay time of the luminophore, the luminescence signal will be out of phase with the excitation light modulated at a

certain frequency. The phase difference β is related to the lifetime τ by the equation $\beta = \tan^{-1}(\omega\tau)$, where ω is the modulation frequency. Thus, the phase difference is a function of temperature and pressure.

Typical relations between lifetime and temperature for EuTTA-dope paint and Ru(bpy)-Shellac paint are shown in Fig. 8. Similar lifetime-temperature relations for different TSPs and thermographic phosphors can be found in the papers by Sholes and Small (1980), Grattan et al. (1987), Bugos (1989) and Noel et al. (1985). In addition, the dependence of the phase difference on temperature for Ru(bpy)-Shellac paint was given by Campbell et al. (1994). For a typical PSP, Ru(ph_2-phen) in GE RTV 118, a lifetime-pressure relation at 22 ^{0}C is shown in Fig. 9. Calibration data follow the Stern-Volmer relation. For a proprietary PSP, Davies et al. (1995) obtained calibration curves of lifetime as a function of pressure and temperature. The Stern-Volmer relations between lifetime and oxygen partial pressure or concentration for several other oxygen sensitive luminescent materials were determined by Gewehr and Delpy (1993), Gord et al. (1995), Sacksteder et al. (1993) and Xu et al. (1994).

5. MEASUREMENT SYSTEMS

The essential elements of the measurement systems for both TSPs and PSPs include illumination sources, optical filters, photodetectors and data acquisition/processing units. This section provides a brief description of four measurement systems: the CCD camera system, the two-color luminophore system, the laser scanning system, and the lifetime (phase) detection system. Each system has advantages over the others and

researchers must choose the one most suitable to meet the specific requirements of their tests.

5.1 CCD camera system

The CCD camera system for luminescent paints is the most commonly used in aerodynamic testing. A schematic of this system is shown in Fig. 10. The luminescent paint (TSP or PSP) is applied to the surface of the model. The paint is excited to luminesce by an illumination source, such as a UV lamp or a laser. The luminescent intensity is filtered optically to eliminate the illuminating light and then captured by a CCD camera and transferred to a computer with a frame grabber board for image processing. Both a wind-on image (at temperature or pressure to be determined) and a wind-off image (at a known constant temperature or pressure) are obtained. In order to correct the dark current dc offset in the CCD camera, a dark current level image is also acquired when no light is incident on the camera. The ratio between the wind-on and wind-off images is taken after the dark current level image is subtracted from both images, yielding a relative luminescent intensity image. Using the calibration relations, the surface temperature or pressure distribution can be computed from the relative luminescent intensity image.

Selection of the appropriate illumination source depends on the absorption spectrum of the paint and the optical access of the facility. The source must provide a large number of photons in the wavelength band of absorption. A variety of illumination sources are available. Lasers with fiber-optic delivery systems have been used in wind tunnel tests (Morris et al. 1993b, Crites 1993, Bukov et al.. 1992, Volan et al. 1991, Engler et al. 1991, 1992). Other light sources reported in the literature include a xenon

arc lamp with a blue filter (McLachlan et al. 1993a), incandescent tungsten/halogen lamps (Dowgwillo et al. 1994) and fluorescent UV lamps (Liu et al. 1995a, 1995b). Morris et al. (1993a) and Crites (1993) discussed the characteristics of some illumination sources. For imaging the surface, scientific grade cooled CCD digital cameras can provide high intensity resolution (12 and 16 bits) and high spatial resolution (up to 2048 × 2048 pixels). Since the scientific grade CCD camera exhibits good linearity and high signal-to-noise ratio (SNR), it is particularly suitable to quantitative luminescent intensity measurements. However, this type of the CCD camera is very costly. A less expensive consumer grade CCD camera can also be used for imaging if the system is carefully calibrated. The low SNR can be greatly improved by averaging a sequence of images (Morris et al. 1993a). When there are large intensity variations over the surface of a model, a consumer grade CCD camera is able to give acceptable quantitative results.

A necessary step in data processing is taking the ratio between the wind-on luminescence image and the wind-off reference image at a known reference temperature or pressure. As indicated in section 2, this ratio process can eliminate the effects of spatial non-uniformity in illumination light, coating thickness, and luminophore concentration. However, since aerodynamic forces may cause model motion and deformation in high-speed wind tunnel tests, the wind-on image may not align with the wind-off image. Thus, the ratio between the non-aligned images can lead to considerable errors in calculating temperature or pressure using the calibration relations. Also, some distinct flow characteristics, such as shock, transition and separation locations, could be smeared. In order to correct this alignment problem, an image registration method was suggested by

Bell and McLachlan (1993) and Donovan et al. (1993). The principle of image registration is based on a mathematical transform that maps the non-aligned and distorted model planform in the wind-on image plane (x', y') onto the reference model planform in the wind-off image plane (x, y). In general, the transform can be written as a power series

$$(x, y) = \left(\sum_{i,j=0}^{m} a_{ij} x'^{i} y'^{j}, \sum_{i,j=0}^{m} b_{ij} x'^{i} y'^{j} \right).$$

Geometrically, the constant terms represent translation, the linear terms represent rotation and scaling, and the non-linear terms represent curvature and higher order corrections. To determine the unknown coefficients a_{ij} and b_{ij}, fiducial marks are placed on the model. The displacement of these marks signifies how the model planform is shifted and deformed. The number of marks needed depends on how many unknown coefficients are to be determined by solving a linear system of algebraic equations such that the mark locations in the wind-on image plane match those in the wind-off image plane. For most wind tunnel tests, a second order transform (m = 2) is sufficient.

Note that image registration is a purely geometric correction method. It fails to take into account differences in illumination light intensity between the wind-off and wind-on cases. The error induced by the variation in illumination level due to model motion is difficult to estimate. An analysis on this issue was given by Bell and McLachlan (1993) in a simplified circumstance. If the illumination light is nearly homogenous and the model displacement is small, the induced errors due to illumination variation should be small.

Tests show that image registration considerably improves the quality of temperature and pressure field images (McLachlan and Bell 1995).

5.2 Two-color luminophore system

The two-color luminophore system is a camera system for a two-color luminescent paint. As mentioned above, the use of the normal CCD camera system requires a ratio between the wind-on and wind-off luminescent images. This image ratio method inevitably causes inaccuracy in determining temperature or pressure, although image registration can be used to correct displacement effects. A two-color luminophore paint would eliminate the need for a wind-off reference image. A two-color luminescent TSP is made by combining a temperature-sensitive luminophore with a temperature-insensitive reference luminophore. Similarly, a two-color luminescent PSP consists of a pressure-sensitive luminophore with a pressure-insensitive reference luminophore. The probe luminophore and reference luminophore can be excited by the same illumination. However, there is ideally no overlap between the emission spectra of the probe luminophore and reference luminophore such that two color luminescent images can be completely separated by optical filters. The ratio between these two images can eliminate effects of spatial non-uniformities in illumination, paint thickness and luminophore concentration. Besides the aforementioned combinations, a temperature sensitive luminophore which is not quenched by oxygen can be combined with an oxygen sensitive luminophore. This dual luminophore temperature/pressure paint can be used for temperature correction in PSP measurements. Furthermore, a multi-color PSP can be

developed to simultaneously correct the effects of both temperature variation and non-uniformities in lighting, paint thickness and concentration.

Some preliminary experiments indicate that a two-color PSP can correct variations in illumination intensity (Oglesby et al. 1995b, Harris and Gouterman 1995). Three pressure sensitive paints with an internal temperature sensitive luminophore have also been tested by Oglesby et al. (1996). These results show that the dual luminophore paint enables point-by-point correction of the temperature effects on PSP measurements. Nevertheless, a two-color PSP has not been used in a wind tunnel test yet. Recently, a two-color PSP was used to measure the pressure distribution in a low speed impinging jet (Torgerson et al. 1996).

In contrast, the two-color thermographic phosphor technique is well developed and has been used at NASA-Langley for aerothermodynamic testing (Buck 1988, 1989, 1991). This system used a 'blue-green' Radelin phosphor that exhibits two emission peaks at 450 nm and 520 nm. It was found that the ratio of the blue to green emission intensities is a function of temperature and independent of the UV illumination intensity. A more current two-color phosphor system uses a 'green-red' mixture of rare-earth and Radelin phosphors for a broader range of temperature sensitivity. Separated filtered images were recorded by three CCD cameras, utilizing off-the-shelf front-end video optics to discriminate wavelengths and align camera images. The blue and green images were digitized by a patented video acquisition system (512 $\times$ 512 pixels) and transferred to workstations for data processing. Surface temperature distributions at different times were calculated using the calibration relation and heat transfer distributions were obtained

based on the one-dimensional heat conduction equation. Detailed descriptions of the multi-color phosphor thermography system are given by Buck (1988, 1989). In principle, this measurement system can also be used for multi-color PSP measurements.

5.3 Laser scanning system

A laser scanning system for TSPs and PSPs is shown in Fig. 11. A low power laser is focused to a small point and scanned over the surface of the model using computer controlled mirrors The laser illumination excites the paint on the model and luminescence is detected by a low noise photodetector (e.g. a PMT). The photodetector signal is digitized with a high resolution A/D converter and processed to obtain temperature or pressure. The mirror is synchronized to the data acquisition so that the position of the laser spot on the model is accurately known. The mirror can be scanned continuously or in steps. In order to compensate for the effect of laser power drift, laser power variation is monitored by a photodiode. Detailed descriptions of the laser scanning system for TSPs and PSPs are given by Hamner et al. (1994), Burns (1995), Torgerson et al (1996) and Torgerson (1996).

Compared with the CCD camera system, the laser scanning system has some advantages. (i) Luminescence is detected by a low noise photodetector. Before the analog output from the PMT is digitized, several SNR enhancement techniques are available to improve the measurement resolution. Amplification and band limited filtering can be used to improve SNR. The signal is then digitized with a high resolution (12 to 24 bit) A/D converter. Additional noise reduction can be accomplished by using a lock-in amplifier if the laser intensity is modulated. (ii) The laser scanning system can be used for

measurements in a facility where optical access is very limited and the CCD camera system is difficult to use. (iii) The system provides uniform illumination over the surface by scanning a single light spot. The laser power is easily monitored and correction for laser power drift can be made for each measurement point. (iv) The system can be easily adapted for measurement of luminescent lifetime or phase shift if a pulsed or modulated laser is used.

5.4 Lifetime-based detection system

A promising method for making temperature and pressure measurements is by determining the luminescent lifetime of the paint rather than the luminescent intensity. Compared with the intensity-based method, the greatest advantage of this method is that the lifetime-temperature or -pressure relation is not dependent on illumination intensity. Therefore, the calibration relation is intrinsic for a particular paint and the intensity ratio process is not required. Also, the lifetime measurement is insensitive to luminophore concentration, paint thickness, photodegradation, turbid paint surface and dirty optical surfaces. The temperature or pressure can be directly obtained from the measured lifetime. The lifetime measurement technique has been well-developed by photochemists (Brody 1957, Bennett 1960, Gewehr and Delpy 1993, Sholes and Small 1980, Grattan et al. 1987, Birch and Imhof 1991, Szmacinski and Lakowicz 1995, Papkovsky 1995). However, a practical lifetime measurement system for aerodynamic testing is still in an initial stage of development. The basic configuration of this system could be similar to the laser scanning system in Fig. 11, except a pulsed excitation light would be used. After each pulse, the luminescence decay is detected by a PMT and acquired by a computer.

The lifetime can be calculated by fitting the data with a single exponential function, or a multi-exponential function for a complex decay. Then, temperature or pressure is obtained using the calibration relation. With thermographic phosphors, Tobin et al. (1990) and Alaruri et al. (1995) have explored the feasibility of the lifetime detection method for temperature measurement on rotating turbine blades. Using a lifetime detection system, Davies et al. (1995) measured the pressure distributions on a cylinder in subsonic flow and on a wedge at Mach 2. Comparison with data obtained by conventional pressure taps was favorable.

A frequency-domain method equivalent to lifetime measurement is detection of the phase angle between the luminescence emission and the modulated excitation light (Birch and Imhof 1991). When harmonic modulation of the illumination light is used, the response of the luminescence intensity can be simply described by a first order model equation, $dI/dt = -I/\tau + A\exp(i\omega t)$, where τ is the lifetime, ω is the angular frequency of modulation, and A is the absorption amplitude of the paint under the modulated excitation light. The solution to this equation is $I = \tau A(1+\omega^2\tau^2)^{-1/2}\exp[i(\omega t - \beta)]$, where $\beta = \tan^{-1}(\omega\tau)$ is the phase angle of the luminescence response with respect to the modulated excitation light. If the modulation frequency is fixed, the phase angle β is a function of the lifetime and hence is dependent on temperature or pressure. The phase angle can be measured using a lock-in amplifier. Campbell et al. (1994) gave a calibration between phase angle and temperature for Ru(bpy)-Shellac paint at 100 kHz modulation frequency. A simple phase detection system using blue LED excitation was used to measure surface temperature on an electrically heated steel foil on which a round air jet

impinged (Campbell et al. 1994). Torgerson et al. (1996) measured the pressure distribution in a low-speed impinging jet using a laser scanning system with an optical modulator. A portable two-dimensional laser scanning system that can simultaneously detect intensity and phase angle is being developed at Purdue University (Torgerson 1996). Recently, the capability of this system was examined by measuring pressure distributions on an airfoil in a transonic wind tunnel. The pressure distributions obtained based on phase detection are in agreement with those obtained based on intensity detection. In future, an improved system will be used to measure the pressure distribution on a wing in flight.

6. ACCURACY

Several papers have addressed the accuracy of the TSP (Liu et al. 1995c, Cattafesta and Moore 1995) and PSP techniques (Morris et al. 1993a, Sajben 1993, Bukov et al. 1993, Crites 1993). In general, the accuracy of the luminescent paint techniques depends on the properties of the paint itself and the measurement system used. The error sources can be divided into three groups. The first class includes the error sources related to the chemical and physical properties of the luminescent paint itself, such as photodegradation, temperature and pressure hysteresis, uncompensated temperature influence, and the induction effect described by Uibel et al. (1993). The second class contains the error sources of the measurement system, such as temporal variation of illumination intensity, photodetector noise (shot noise and Johnson noise), photodetector dark current, non-linearity of photodetector response, non-uniformity of CCD array,

wavelength overlap between illumination source and optical filters, and ambient light. The third class of errors originates from displacement and deformation of the model due to aerodynamic forces, contamination of the painted surface during wind tunnel tests, and luminescence scattering interference between neighboring surfaces of a complicated model configuration. Most of these errors are systematic errors and some, such as photodetector noise and random variation of illumination intensity, are random errors. Since the luminescent paint method is comprised of many different technical components, a complete error analysis is a difficult task. Nevertheless, an effort has been made to understand these error sources.

For TSPs, some of the systematic error sources can be controlled and compensated. The effect of photodegradation can be minimized by reducing exposure time. For some TSP coatings, the effect of temperature hysteresis (a phenomenon related to the polymer structural transformation from a brittle glassy state to a soft rubbery state) can be eliminated by pre-heating the paint beyond the glass temperature (Liu et al. 1995c, 1996b, Romano et al. 1989). After minimizing exposure time and removing temperature hysteresis effects, Liu et al. (1995c, 1996b) repeated calibration tests over several different days for two typical TSPs (EuTTA-dope paint and Ru(bpy)-Shellac paint) using the apparatus shown in Fig. 2. The frequency distributions of temperature error are shown in Fig. 12 for these TSPs. A Gaussian distribution is also plotted as a reference. The standard deviation of the temperature error is about $\pm$ 0.8 ^{0}C for EuTTA-dope paint and about $\pm$ 2 ^{0}C for Ru(bpy)-Shellac paint. This calibration uncertainty includes the contributions from random error sources related to the measurement system and the paint

itself. Hence, the results of these repeated measurements provide an understanding of the uncertainty in TSP measurements. The largest discrepancies often occur at higher temperatures where the luminescence is weak and the signal-to-noise ratio is low.

In order to evaluate the noise level of a scientific-grade CCD camera system, Cattafesta and Moore (1995) examined the temperature uncertainty distribution on an iso-thermal swept cylinder with a proprietary TSP coating. Actually, this uncertainty is dominated by random errors of the CCD camera and represents a limit of achievable temperature resolution of the measurement system. The uncertainty was found to vary from 0.23 ^{0}C to 0.57 ^{0}C. Furthermore, to assess the bias error due to model motion, the swept cylinder was slightly deflected (less than one pixel) by loading the model with weights. A simulated wind-on image was acquired. In this case, the uncertainty varied from 0.23 ^{0}C to 4 ^{0}C. The larger error occurs at the edges of the model as a result of the model motion. Liu (1996b) estimated the noise level of a standard CCD camera system and a laser scanning system by determining the temperature on an iso-thermal surface with EuTTA-dope and Ru(bpy)-Shellac paints. Improvements in SNR for these systems can be achieved by ensemble averaging and using a lock-in amplifier.

For a PSP measurement system, the uncertainty in pressure can be determined through repeated calibration tests. Using a simple calibration system with Argon laser excitation and a PMT, calibration tests were repeated for a PSP sample (Ru(ph_2-phen) in GE RTV 118) at ambient temperature over several different days. Figure 13 shows the frequency distribution of pressure error. The standard deviation is 0.2 psid over a pressure range from 3 to 14.5 psia. In the above tests, daily temperature fluctuations may

contribute significantly to calibration error since temperature in the vacuum chamber was not controlled. It is expected that the uncertainty can be reduced in well-controlled testing conditions. To estimate the uncertainty of PSP measurement with a scientific-grade CCD camera system, Morris et al. (1993a) conducted a series of calibration experiments focused on a proprietary PSP paint sample in a temperature and pressure controlled vessel. After averaging 32 sequential images to improve SNR, they found that the minimum pressure resolution near atmospheric pressure (13 to 16 psia) is about $\pm$ 0.05 psid for their system. Note that the above uncertainty estimates do not contain the contributions from some major error sources such as temperature effects and model displacement. The uncertainty of PSP measurements depends strongly on a systematic error source associated with the temperature dependence of the paint. An analysis by Sajben (1993) indicates that without implementing correction, temperature effects may result in large errors in PSP measurements on a strongly non-isothermal surface.

7. TIME RESPONSE

In short-duration wind tunnel tests and for unsteady flow measurements, fast time response of the luminescent paint is desirable. There are two characteristic time scales that are related to the time response of the paint system. One is the luminescent lifetime which represents an intrinsic physical limit for the achievable temporal resolution of the paint. Luminescent paints usually have a lifetime ranging from 10^{-10} seconds to milliseconds. Another is the time scale of the diffusion processes: thermal diffusion for a TSP layer and oxygen diffusion for a PSP layer. Based on the transient solution of the

diffusion equation, the oxygen diffusion time for a thin PSP coating is on the order of L^2 / D_m, where L is the coating thickness and D_m is the mass diffusivity. Similarly, the thermal diffusion time for a thin TSP coating is on the order of L^2 / α, where α is the thermal diffusivity. In a forced-convection-dominated case, the thermal diffusion time can also be expressed by $Lk / \alpha h$, where k is the thermal conductivity and h is the convection heat transfer coefficient. In general, the diffusion time is much larger than the lifetimes of most luminescent paints. Therefore, the time response of a luminescent paint is mainly limited by the diffusion processes for both TSP and PSP measurements.

To evaluate the time response of a TSP coating to a rapid temperature rise, Liu et al. (1995c) conducted a pulsed laser heating experiment. One side of a 25 μm thick steel foil was heated by a 532 nm pulsed green beam from a Nd:YAG laser. The other side of the foil was coated with Ru(bpy)-Shellac paint (about 10 μm thick) which was excited by a 457 nm blue beam from an Argon laser. The change in luminescence intensity of the paint was detected by a PMT and the temperature response was calculated using the calibration relation. Figure 14 shows a typical temperature response of the paint to the pulsed laser heating. The surface temperature increases rapidly after the pulsed laser beam is turned on and then gradually decays due to natural convection. Two asymptotic solutions for the spatially-averaged temperature increment $< \theta > = < T - T_{in} >$ are obtained. For the rapid heating process, $< \theta > = A_m \, \mathrm{erfc}(\sqrt{\tau_1 / t})$, where $A_m = P\alpha/kL$ and P is the strength of the pulsed heat source. The heating time constant is $\tau_1 = L^2/4\alpha$, where α is the thermal diffusivity and L is the paint thickness. For the temperature decay process, $< \theta > = A_m \exp(-2t / \tau_2)$. The decay time constant $\tau_2 = Lk/\alpha h$, where h is the

heat transfer coefficient of natural convection and k is the thermal conductivity. By fitting the experimental data with the asymptotic solutions, it is found that τ_1 = 0.25 ms and τ_2 = 25 ms. Step-like jet impingement cooling on the surface of a hot body was also used to test the time response of the paint. The time constant $Lk/\alpha h$ depends on the paint thickness and the convection heat transfer coefficient. For the 19 μm thick Ru(bpy)-Shellac paint, the measured time constant is 16 ms for air jet impingement cooling and 1.4 ms for Freon jet impingement cooling, respectively. Clearly, the time constant of the paint is a function of local convective heat transfer.

Baron et al. (1993) studied the time response of several PSPs to oxygen concentration changes using a pressure jump apparatus. The major component of their apparatus is an air-tight chamber in which the PSP sample is located. After the chamber is sufficiently evacuated, a valve is opened such that the pressure inside the chamber changes from near vacuum to ambient pressure in about 1 ms. The corresponding luminescence intensity change is detected by a PMT. Then, the response time is calculated. The PSPs that they investigated are PtOEP in GP-197 and MAX-100 polymer binders and H_2TFPP in Silica-W, Silica-B and TLC binders. They found that the response times for the GP-197 and MAX-100 binders are 2.45 s and 0.4 s, respectively. The Silica-W and Silica-B samples showed response times of 11 ms and 1.5 ms, respectively. The response time of the TLC sample was about 25 μs. Recently, using a similar set-up, Carroll et al. (1996) measured the response of three PSPs to a step input: a proprietary PSP from McDonnell Douglas, PtOEP on a white primer layer, and PtOEP in GP-197. For the McDonnell Douglas paint with thickness ranging from 13 to 35 μm, the response time varied from

0.042 s to 0.42 s. The response time of PtOEP on a white primer layer was found to be 45 ms. For PtOEP in GP-197, the response times were 1.4 s, 1.6 s and 2.6 s for paint thickness of 22 μm, 26 μm and 32 μm, respectively. Typical responses of PtOEP in GP-197 to a step pressure jump are shown in Fig. 15. In addition, the response of PtOEP in GP-197 to a sinusoidal pressure field was investigated by Carroll et al. (1995). The PSP response amplitude and phase shift behave like a first-order linear system with a time constant on the order of 1 s. The PSP response was further studied by Winslow et al. (1996) in the frequency domain. Engler (1995) also tested the PSP response to periodic pressure changes. For this paint, the limit of the frequency response was about 50 Hz and therefore the time constant was about 20 ms. Bukov et al. (1992) reported that a proprietary fast-responding PSP coating developed by TsAGI has a time constant of 5 ms. Clearly, the diverse time constants of various PSPs result from effects of the different polymer diffusivity, coating thickness and structure of the paints. In addition, Coyle et al. (1995) noted that the basecoat on which the PSP is applied may increase the response time through interactions between the basecoat and the paint (oxygen degassing and solvent attack).

8. TSP APPLICATIONS

The TSP technique has been used in wind tunnel tests for flow diagnostics and for measuring heat transfer. This section briefly describes several typical applications of TSP.

8.1 Hypersonic vehicle models

Global surface heat transfer distributions on a waverider model in Mach 10 flow have been obtained using EuTTA-dope paint (Liu et al. 1994b, 1995b). These experiments were conducted in the Hypervelocity Wind Tunnel No. 9 at the Naval Surface Warfare Center. The waverider model has an overall length of 39 inches, a span of about 16.2 inches and a base height of about 6.8 inches. The angle of attack was 10 degrees and the wind tunnel run time was 2.3 seconds. A thin Mylar insulating layer covered one half of the windward side of the model, and EuTTA-dope paint was applied on the insulating layer. The temporal evolution of the surface temperature distribution was obtained, and then heat flux was calculated using a simple heat transfer model. Figure 16 shows a representative map of heat flux on the windward side of the waverider model when time is 0.57 seconds from tunnel start-up. The bright and dark regions correspond to high and low heat transfer, respectively. The low heat transfer region near the leading edge corresponds to laminar flow. Transition from laminar to turbulent flow can be easily identified by an abrupt change from low to high heat transfer. Also observed was movement of the transition line toward the leading edge as the laminar region diminished and the surface temperature increased with time. Figure 17 shows a typical heat transfer history for one location on the model. The TSP measurement is in good agreement with data obtained by thermocouples.

Two-color phosphor thermography has been developed at NASA-Langley to assess the aerodynamic heating on hypersonic vehicles (Buck 1988, 1989, 1991). Figure 18 shows a sample temperature image on a candidate vertical takeoff/vertical lander concept. The configuration forebody is a sphere-cone with an 8 degree half angle.

Toward the rear of the configuration, the cone intersects a cylinder with four flats cut on it around the circumference. On each flat, a control flap has been positioned. The model was tested in Langley's 20-in Mach 6 tunnel. For the images shown here, the camera is viewing the windward side of the model. The model is at an angle of attack of 17.5 degrees, the body flap is deflected 20 degrees and the freestream Reynolds number is 7.35 million per foot. The phosphor image exhibits a high heating front proceeding from the side of the cone back to the centerline. The high heating is associated with the onset of crossflow transition. Another example is a 0.75% scale Shuttle Orbiter model. A temperature image of the windward side of the model is shown in Fig. 19. This experiment investigated the sensitivity of transition to roughness height and off-centerline location. The model is at 40 degrees angle of attack, the body flap and elevon deflection angles are zero, Mach number is 6 and the freestream Reynolds number is 3 million per foot. A small roughness element, approximately scaled to resemble a raised shuttle tile, is located on the windward side at a quarter of the body length from the nose. The phosphor image clearly shows the turbulent wedge caused by the tripping element.

8.2 Shock/boundary layer interaction

EuTTA-dope paint has been used to measure heat transfer in several typical shock/turbulent boundary layer interacting flows: swept shock/boundary layer interaction, flows over rearward- and forward-facing steps, and incident shock/boundary layer interaction (Liu et al. 1995a). The field mapping ability of the TSP technique allows the study of heat transfer patterns in three-dimensional separated flows induced by shock/boundary layer interactions. A typical test example is the swept shock/turbulent

boundary layer interaction. An attached planar shock generated by a sharp fin interacts with an incoming turbulent boundary layer on the floor of the test section and produces a complicated three-dimensional flow separation. Previous experiments (Settles and Lu 1985) suggested that except in the inception region near the leading edge of the fin, physical quantities (pressure, heat transfer, etc.) on the floor may approach a quasi-conical symmetrical state in which these quantities remain invariant along a ray from a virtual conical origin. Several heat transfer measurements (Lee and Settles 1992, Rodi and Dolling 1992) were made in the quasi-conical symmetry region using conventional sensors distributed discretely along a fixed arc. The TSP coating allows heat transfer measurement in the inception region where flow lacks the presumed quasi-conical symmetry and heat transfer significantly changes along the radial direction. Figure 20 shows a heat transfer map in the inception region which was obtained from a luminescent intensity image at $M_\infty = 2.5$, $\alpha = 10^0$ and $Re_\delta = 1.3 \times 10^5$. In the map, bright and dark regions correspond to high and low heat transfer, respectively. The primary separation line can be identified. The highest heat transfer region is located in the neighborhood of the fin. Figure 21 presents the distributions of the relative Stanton number St/St_r along four circular arcs with different radial distance R from the leading edge of the fin, where St_r is a reference Stanton number in the undisturbed boundary layer upstream of the leading edge. As R increases, the distributions tend to approach an asymptotic profile near the fin while the asymptotic tendency is quite evident near the inviscid shock location. When the maximum relative Stanton number St_{max}/St_r is taken as a characteristic quantity, it is found that St_{max}/St_r increases with the non-dimensional radial distance R/δ and

approaches the value measured in the quasi-conical symmetry region (Lee and Settles 1992). Hence, the asymptotic behavior of heat transfer in the inception region seems to support the concept of quasi-conical symmetry.

8.3 Boundary layer transition detection

TSP has also been utilized as an approach to flow transition detection (Campbell et al. 1992, Campbell 1993, McLachlan et al. 1993b). Since convective heat transfer is much higher in turbulent flow than in laminar flow, TSP can visualize the surface temperature difference between laminar and turbulent regions. In low speed wind tunnel tests, the model is typically heated or cooled to enhance temperature variation across the transition line. However, in high Mach number wind tunnel tests, artificial heating is not necessary since skin friction can produce a significant temperature difference between laminar and turbulent flow regions. Using EuTTA-dope paint, Campbell et al. (1992, 1993) visualized transition patterns on a Boeing symmetric airfoil and a symmetric NACA 65_4-021 airfoil in a low-speed wind tunnel. The dependence of transition location on the angle of attack was also determined. In these experiments, the models were pre-heated to about 50 ^{0}C with a spot lamp in order to produce a temperature difference between turbulent and laminar flow regions during subsequent convection cooling. A similar transition detection experiment for a NACA-64A010 airfoil was carried out by McLachlan et al. (1993b) using a proprietary TSP.

Recently, a cryogenic TSP system has been developed at Purdue University. Several TSP formulations have been successfully used to detect transition on airfoils in a 0.1 m transonic cryogenic wind tunnel at the National Aerospace Laboratory (NAL) in

Japan and a 0.3 m cryogenic wind tunnel at NASA-Langley. In the NAL tests, two formulations, Ru(trpy)-GP197 and Ru(VH127)-GP197, were used in a temperature range from 90 to 150 K (Asai et al. 1996). The NACA 64A012 airfoil models were made of white glass ceramic (MACOR) and stainless steel. The stainless steel model was covered with a thin white Mylar insulating layer in order to increase surface temperature variation. In these tests, the total temperature varied from 90 to 150 K, the Mach number from 0.4 to 0.7 and the Reynolds number based on chord from 2.2 to 8.5 million. In order to enhance the temperature difference across the transition line, both a transient method of rapidly changing the freestream temperature and a steady internal heating method were employed. The effects of Reynolds number on transition pattern were also examined. Figure 22 shows a typical relative luminescent intensity image of Ru(VH127)-GP197 paint on the MACOR airfoil model at Mach 0.4 and a total temperature of 150 K. Flow is from left to right. Bright and dark regions represents high and low heat transfer, respectively. The turbulent wedge induced by a small roughness element placed near the leading edge is clearly visible. The natural transition line near the trailing edge is also apparent. Quantitatively, surface temperature can be calculated from the luminescent intensity ratio using the calibration relation. Figure 23 shows the chordwise surface temperature distributions at natural and forced transition locations on a stainless steel model with a thin insulating layer. For this test, the freestream total temperature was rapidly changed from 150 to 142.5 K using liquid nitrogen injection. Natural transition is signified by a sudden decrease in the chordwise temperature distribution. These results indicate that the TSP

technique is a promising method for transition detection at cryogenic conditions where many methods do not work.

8.4 Heat transfer in an excited circular impinging jet

Heat transfer distributions in an acoustically excited impinging jet were recently investigated by Liu and Sullivan (1996a) using the TSP technique. A circular air jet impinged on a thin stainless steel sheet stretched taut with springs and heated uniformly by an electric current. EuTTA-dope paint was applied to the back side of the steel sheet for temperature mapping. Two-dimensional Nusselt number distributions were obtained for different excitation frequencies. These heat transfer distributions were affected by forcing the impinging jet, and the local heat transfer in the wall jet region was either enhanced or reduced by adjusting the excitation frequency. The relationship between local heat transfer and large-scale organized vortical structures was also explored.

8.5 Surface temperature of a hot film in shear flow

Using an optical magnification system, the TSP technique can achieve a very high spatial resolution over the surface of a small object. The TSP method has been used to measure the surface temperature field of a flush-mounted hot film sensor in a turbulent boundary layer on a flat plate (Liu et al. 1994a). A commercial hot film sensor (TSI 1237), which has a 0.127 mm streamwise length and a 1 mm spanwise length, was studied. EuTTA-dope paint was applied to the hot film sensor for temperature mapping. Luminescence intensity images were obtained with a camera through an optical magnification system. Streamwise and spanwise surface temperature distributions were computed from the intensity images.

9. PSP APPLICATIONS

Most PSP measurements on aerodynamic models have been conducted in transonic and supersonic wind tunnels. Recently, the PSP technique has been used for pressure measurements in low-speed flows and on rotating machinery.

9.1 Tests in wind tunnels

PSPs have been applied to pressure measurements in wind tunnel tests over a wide range of Mach numbers in order to examine the feasibility of this method. Kavandi et al. (1990) and McLachlan et al. (1993a) tested a two-dimensional airfoil (NACA-0012) over a Mach number range of 0.3 to 0.66. A shock on the model upper surface was clearly identified at a Mach number of 0.66. Comparison of the PSP pressure results to conventional pressure tap measurement was good. McLachlan et al. (1995a, 1995b) also tested a large generic transport wing/body configuration at transonic Mach numbers from 0.7 to 0.9. The PSP data not only provide good quantitative chordwise pressure results, but also give complicated two-dimensional pressure maps that would be difficult to deduce from the usual discrete tap data. Some experiments conducted in the McDonnell Douglas Research Laboratories (Morris et al. 1993b) include pressure measurements on a generic wing/body model ($M_\infty = 2$ and $\alpha = 8$ degrees), a model of a high performance fighter ($M_\infty = 1.2$), and a two-dimensional converging/diverging nozzle. The McDonnell Douglas PSP was also used to visualize the pressure distribution in a shock/turbulent boundary layer interaction (Donovan 1992, Morris et al. 1993b) and measure the pressure field about a sonic jet injected transversely into a Mach 1.6 free-stream flow (Everett et al.

1995). Sellers and Brill (1994) conducted a demonstration test of a PSP on an aircraft model in the Arnold Engineering Development Center transonic wind tunnel. The PSP data agrees well with conventional pressure measurements and CFD computations. Some experiments have also been done in short-duration wind tunnels. Using fast-responding PSP coatings developed at TsAGI, Troyanovsky et al. (1993) carried out a semi-quantitative pressure visualization for a shock/body interaction in a Mach 8 shock tube with 0.1 s duration, and Borovoy et al. (1995) determined the pressure distributions on a cylinder at Mach 6 in a shock wind tunnel with about 40 ms duration. In general, the PSP technique works well in high Mach number subsonic flows and supersonic flows since static pressure changes are typically large. Recently, Morris (1995) measured the pressure distributions on delta wings at low Mach numbers ranging from 0.05 to 0.2. These results indicate the low pressure regions induced by leading edge vortices. Good quantitative agreement is shown between the paint measurements and tap measurements.

Figure 24 shows a typical surface pressure map for the interaction of a cylinder mounted normal to a flat floor with a supersonic turbulent boundary layer at a freestream Mach number of 2.5. In this test carried out in the Purdue University supersonic wind tunnel, the incoming boundary layer thickness is 4 mm, the cylinder height is 15 mm, and the cylinder diameter is 4.8 mm. The viewing angle of the camera is about 50 degrees. The PSP, Ru(ph_2-phen) in GE RTV 118, was applied to the floor surface for pressure measurement. The pressure map clearly indicates a pressure rise induced by a bow shock ahead the cylinder and a low pressure region in the turbulent wake behind the cylinder. The centerline pressure distribution ahead of the cylinder is plotted in Fig. 25 along with

pressure tap data. The general behavior of the pressure distribution agrees with the previous results of Dolling and Bogdonoff (1981).

9.2 Tests in rotating machinery

The PSP technique provides a promising tool for measuring surface pressure distributions on a high-speed rotating blade with high spatial resolution. Instrumentation is particularly difficult in the rotating environment. The conventional pressure taps give pressure data only at discrete points and weaken the structure of the rotating blade. In contrast, the PSP method does not have these disadvantages since the sensor coating is applied to the blade surface and the luminescence measurement is non-contact. Preliminary PSP measurements on rotating machinery were conducted by Burns and Sullivan (1995) with a laser scanning system. Using Green Gold absorbed onto silica gel TLC plates, pressure distributions were obtained on a small wooden propeller (37 cm radius and 3.8 cm chord) at a rotational speed of 3120 rpm and a TRW Hartzell propeller (92 cm radius and 10.4 cm chord) at a rotational speed of 2360 rpm. The PSP-derived pressure coefficient distributions across the blade show a reasonable trend. Instead of a laser scanning system, Hubner et al. (1996) suggested a lifetime imaging method for pressure measurements on rotating machinery. This method is based on detecting the luminescent decay traces of a rotating painted surface on a CCD camera. Recently, a test was performed to measure the chordwise pressure distributions on the rotor blades of a high speed axial flow compressor (Liu et al 1997). TSP (Ru(bpy)-Shellac) and PSP ($Ru(ph_2$-phen) + silica gel particles in GE RTV 118) were applied to alternating blades. The TSP provided the temperature distributions on the blades for temperature correction

of the PSP results. A scanning laser system was used for excitation and detection of luminescence. Both the TSP and PSP were excited with an Argon laser and luminescence was detected with a Hamamatsu PMT. The laser scanned 21 spanwise locations over 2 inches on each blade. At each spanwise location, data was acquired at 100 chordwise locations over 2 inches. Thus, two-dimensional temperature and pressure maps at different rotational speeds were obtained on the blade surfaces. Figure 26 shows the chordwise pressure distributions on the suction side of a rotating blade at a radius of 5 inches (mid-span) for several rotational speeds (10000, 13500, 14750, 16000, 17000, and 17800 rpm). The pressure distributions indicate the formation of a shock on the surface as rotational speed is increased. The rapid rise in surface pressure induced by the shock can be clearly observed at the high rotational speeds of 16000, 17000 and 17800 rpm.

10. CONCLUSIONS

The fundamentals of the TSP and PSP techniques have been discussed in this review. The TSP technique has been used not only to visualize surface flow features such as boundary layer transition, shocks and separation, but also to obtain quantitative surface temperature and heat transfer maps in several cases with good accuracy. Applications of the PSP technique are focused on surface pressure measurements on airfoils, generic wing-body models and aircraft models over a wide range of Mach numbers. The field mapping capability of the TSP and PSP techniques provides information about complicated flow characteristics that cannot be easily acquired using more conventional methods. Much effort has being made to improve the essential elements of the

measurement system including paint formulation, illumination, imaging, and data acquisition/processing hardware and software. Currently, the development of successful TSP and PSP formulations is of fundamental importance. While no single TSP or PSP is applicable to all test conditions, a series of optimal TSPs and PSPs will be developed in the future for temperature and pressure measurements in most wind tunnels ranging from cryogenic to high enthalpy tunnels encompassing subsonic to hypersonic speeds. The capability of the measurement systems can be further extended and refined such that TSP and PSP measurements will become a routine procedure in aerodynamics testing.

Acknowledgment:

This work was supported by ONR, AFOSR, NASA Langley, NASA Ames, NASA Lewis and the Boeing Company. The authors would like to thank G. Buck, N. R. Merski, S. A. Berry, and G. Brauckmann of NASA Langley for providing heat transfer and temperature images. Thanks are also due to B. F. Carroll of the University of Florida for providing his figure of the step response of a PSP. We also thank Shad Torgerson, who provides data for Fig. 26 and is currently developing a two-dimensional laser scanning system for TSPs and PSPs at Purdue University. We are also thankful to the four reviewers for their constructive comments.

REFERENCES

Alaruri, S., McFarland, D., Brewington, A. Thomas, M. and Sallee, N. (1995), Development of a Fiber-Optic Probe for Thermographic Phosphor Measurements in Turbine Engines, Optics and Lasers in Engineering 22, 17-31.

Ardasheva, M. M., Nevskii, L. B. and Pervushin, G. E. (1985), Measurement of Pressure Distribution by Means of Indicator Coatings, Journal of Applied Mechanics and Technical Physics, No. 4, 24-33.

Asai, K., Kanda, H., Kunimasu, T., Liu, T. and Sullivan, J. (1996), Detection of Boundary-Layer Transition in a Cryogenic Wind Tunnel by Using Luminescent Paint, AIAA Paper 96-2185.

Babinsky, H. and Edwards, J. A. (1993), The Application and Analysis of Liquid Crystal Thermographs in Short Duration Hypersonic Flow, AIAA Paper 93-0182.

Baron, A. E., Danielson, J. D., Gouterman, M., Wan, J., Callis, J. B. and McLachlan, B. (1993), Submillisecond Response Times of Oxygen-Quenching Luminescent Coatings, Rev. Sci. Instrum. 64(12), 3394-3402.

Becker, R. S. (1969), Theory and Interaction of Fluorescence and Phosphorescence, Wiley Interscience, New York.

Bell, J. H. and McLachlan, B. G. (1993), Image Registration for Luminescent Paint Sensors, AIAA Paper 93-0178.

Bennett, R. G. (1960), Instrument to Measure Fluorescence Lifetimes in the Millimicrosecond Region, Rev. Sci. Instrum. 31(12), 1275-1279.

Bennett, R. G. and McCartin, P. J. (1966), Radiationless Deactivation of the Fluorescent State of Substituted Anthracences, The Journal of Chemical Physics, Vol. 44, No. 5, 1969-1973.

Birch, D. J. S. and Imhof, R. E. (1991), Time-Domain Fluorescence Spectroscopy Using Time-Correlated Single-Photon Counting, Topics in Fluorescence Spectroscopy, Volume 1: Techniques, edited by J. R. Lakowicz, Plenum Press, New York, Chapter 1.

Borovoy, V., Bykov, A., Mosharov, V., Orlov, A., Radchenko, V. and Phonov, S. (1995), Pressure Sensitive Paint Application in Shock Wind Tunnel, Proc. 16th Int. Cong. Instrumentation in Aerospace Simulation Facilities (ICIASF), Institute of Electrical and Electronics Engineers, Wright-Patterson Air Force Base, Dayton, OH, USA, 34.1-34.4.

Bradley, L. C. (1953), A Temperature-Sensitive Phosphor Used to Measure Surface Temperature in Aerodynamics, Rev. Sci. Instrum. 24(3), 219-220.

Brody, S. S. (1957), Instrument to Measure Fluorescence Lifetimes in the Millimicrosecond Region, Rev. Sci. Instrum. 28(12), 1021-1026.

Buck, G. M. (1988), An Imaging System for Quantitative Surface Temperature Mapping Using Two-Color Thermographic Phosphors, presented at 34th International Instrumentation Symposium, Albuquerque, NM.

Buck, G. M. (1989), Automated Thermal Mapping Techniques Using Chromatic Image Analysis, NASA TM 101554.

Buck, G. M. (1991), Surface Temperature/Heat Transfer Measurement Using a Quantitative Phosphor Thermography System, AIAA Paper 91-0064.

Buck, G. M. (1994), Simultaneous Luminescence Pressure and Temperature Measurements on Dyed Ceramic Models for Hypersonic Wind Tunnels, AIAA Paper 94-2482.

Bugos, A. R. (1989), Characterization of the Emission Properties of Thermographic Phosphors for Use in High Temperature Sensing Applications, M. S. Thesis, The University of Tennessee, Knoxville, Tennessee.

Bukov, A. P., Orlov, A. A., Mosharov, V. E., Radchenko, V. N. and Pesetsky, V. A. (1992), Application of Luminescence Quenching for Pressure Field Measurements on the Model Surface in Wind Tunnel, Proc. Wind Tunnels and Wind Tunnel Test Techniques Conf., Royal Aeronautical Society, London, U. K., pp. 8.1-8.11.

Bukov, A., Mosharov, V., Orlov, A., Pesetsky, V., Radchenko, V., Phonov, S., Matyash, S., Kuzmin, M. and Sadovsky, N. (1993), Optical Surface Pressure Measurements: Accuracy and Application Field Evaluation, 73th AGARD Fluid Dynamics Panel Meeting and Symposium on Wall Interference, Support Interference and Flow Field Measurements, Brussels, Belgium.

Burns, S. (1995), Fluorescent Pressure Sensitive Paints for Aerodynamic Rotating Machinery, M. S. Thesis, School of Aeronautics and Astronautics, Purdue University, West Lafayette, IN.

Burns, S. and Sullivan, J. (1995), The Use of Pressure Sensitive Paints on Rotating Machinery, Proc. 16th Int. Cong. Instrumentation in Aerospace Simulation Facilities (ICIASF), Institute of Electrical and Electronics Engineers, Wright-Patterson Air Force Base, Dayton, OH, USA, 32.1-32.14.

Campbell, B., Liu, T. and Sullivan, J. (1992), Temperature Measurement Using Fluorescent Molecules, Sixth Int. Symp. Appl. Laser Techniques Fluid Mech., Lisbon, Portugal.

Campbell, B. (1993), Temperature Sensitive Fluorescent Paints for Aerodynamics Applications, M. S. Thesis, School of Aeronautics and Astronautics, Purdue University, West Lafayette, IN.

Campbell, B., Liu, T. and Sullivan, J. (1994), Temperature Sensitive Fluorescent Paint Systems, AIAA Paper 94-2483.

Carroll, B. F., Winslow, A., Abbitt, J., Schanze, K. and Morris, M. (1995), Pressure Sensitive Paint: Application to a Sinusoidal Pressure Fluctuation, 16th Int. Cong. Instrumentation in Aerospace Simulation Facilities (ICIASF), Institute of Electrical and Electronics Engineers, Wright-Patterson Air Force Base, Dayton, OH, USA, 35.1-35.6.

Carroll, B. F., Abbitt, J. D., Lukas, E. W. and Morris, M. J. (1996), Step Response of Pressure Sensitive Paints, AIAA J, Vol. 34, No. 3, 521-526.

Cattafesta III, L. N. and Moore, J. G. (1995), Uncertainty Estimates for Luminescent Temperature-Sensitive Paint Intensity Measurements, AIAA Paper 95-2193.

Coyle, L. M., Bullock, J. P. and Gouterman, M. (1995), Interfacial Effects at the Basecoat-PSP Boundary, Abstract of Workshop on Pressure, Temperature and Shear Sensitive Coatings, University of Florida, Gainesville, Florida, USA.

Crites, B. C. (1993), Measurement Techniques ---- Pressure Sensitive Paint Technique, Lecture Series 1993-05, von Karman Institute for Fluid Dynamics.

Crovini, L. and Fernicola, V. (1992), An Oven to Test Fluorescent-Decay Temperature Sensor, Sensors and Actuators B, 7, 529-532.

Czysz P. and Dixon W. P. (1969), Quantitative Heat Transfer Measurement Using Thermographic Phosphors, SPIE Journal, Vol. 7, No. 3, 77-79.

Davies, A. G., Bedwell, D., Dunleavy, M. and Brownjohn, N. (1995), Pressure Sensitive Paint Measurements Using a Phosphorescence Lifetime Method, presented at Seventh International Symposium on Flow Visualization, September 11-14, Seattle, Washington.

Dolling, D. S. and Bogdonoff, S. M. (1981), Scaling of Interactions of Cylinders with Supersonic Turbulent Boundary Layers, AIAA J., Vol. 19, No. 5, 655-657.

Donovan, J. F. (1992), Preliminary Results From a Trangentially Injected Shock Wave/Turbulent Boundary Layer Interaction, presented at 13th Symposium on Turbulence, Rolla, MO.

Donovan, J. F., Morris, M. J., Pal, A., Benne, M. E. and Crites, R. C. (1993), Data Analysis Techniques for Pressure- and Temperature-Sensitive Paint, AIAA Paper 93-0176.

Dowgwillo, R. M., Morris, M. J., Donovan, J. F. and Benne, M. E. (1994), The Application of The Pressure Sensitive Paint Technique to High Speed Wind Tunnel Testing of a Fighter Aircraft Configuration With Complex Store Loadings, AIAA Paper 94-1932.

Engler, R. H., Hartmann, K. and Schultze, B. (1991a), Aerodynamic Assessment of an Optical Pressure Measurement System (OPMS) by Comparison with Conventional Pressure Measurements in a High Speed Wind Tunnel, Proc. 14th Int. Cong.

Instrumentation in Aerospace Simulation Facilities (ICIASF), Institute of Electrical and Electronics Engineers, Rockville, MD, pp. 17-24.

Engler, R. H., Hartmann, K., Troyanovski, I. and Vollan, A. (1991b), Description and Assessment of a New Optical Pressure Measurement System (OPMS) Demonstrated in The High Speed Wind Tunnel of DLR in Gottingen, DLR Report DLR-FB 92-24.

Engler, R. H. (1995), Further Developments of Pressure Sensitive Paint (OPMS) for Non Flat Models in Steady Transonic Flow and Unsteady Conditions, Proc. 16th Int. Cong. Instrumentation in Aerospace Simulation Facilities (ICIASF), Institute of Electrical and Electronics Engineers, Wright-Patterson Air Force Base, Dayton, OH, USA, 33.1-33.8.

Everett, D. E., Dutton, J. C. and Morris, M. J. (1995), Pressure Sensitive Paint Measurements of the Pressure Field about a Sonic Jet Injected Transversely into a Mach 1.6 Free Stream, AIAA Paper 95-0524.

Fried, J. R. (1995), Polymer Science and Technology, Prentice Hall, New York.

Gallery, J. M. (1993), Luminescence Imaging for Aerodynamic Temperature and Pressure Measurements, Ph. D. Thesis, Department of Chemistry, University of Washington, Seattle, Washington.

Gartenburg, E. and Robert, A. S. (1991), Twenty-Five Years of Aerodynamic Research with Infrared Imaging, A Survey, Presented at Thermosense XIII, Int. Conf. Thermal Applications and Image Diagnostic, Orlando, FL.

Gewehr, P. M. and Delpy, D. T. (1993), Optical Oxygen Sensor Based on Phosphorescence Lifetime Quenching and Employing a Polymer Immobilised Metalloporphyrin Probe, Medical & Biological Engineering & Computing, January, 2-21.

Gord, J. R., Buckner, S. W. and Weaver, W. L. (1995), Dissolved Oxygen Quantitation in Fuel Through Measurements of Dynamically Quenched Fluorescence Lifetime, Proc. 16th Int. Cong. Instrumentation in Aerospace Simulation Facilities (ICIASF), Institute of Electrical and Electronics Engineers, Wright-Patterson Air Force Base, Dayton, OH, USA, 39.1-39.6.

Gouterman, M., Callis, J., Burns, D., Kavandi, J., Gallery, J., Khalil, G., Green, E., McLachlan, B. and Crowder, J. (1990), Luminescence Imaging for Aerodynamic Testing, Proc. of the ONR/NASA Workshop on Quantitative Flow Visualization (J. Sullivan and B. Holmes), Purdue University, IN, USA.

Grattan, K. T. V., Palmer, A. W. and Willson, C. A. (1987), A Miniaturised Microcomputer-Based Neodymium'Decay-Time' Temperature Sensor, J. Phys. E: Sci. Instrum. 20, 1201-1205.

Hamner, M., Campbell, B., Liu, T. and Sullivan, J. (1994), A Scanning Laser System for Temperature and Pressure Sensitive Paint, AIAA Paper 94-0728.

Harris, J. and Gouterman, M. (1995), Referenced Pressure Sensitive Paint, Flow Visualization VII, Proceeding of the Seventh International Symposium on Flow Visualization, edited by J. Crowder, Seattle, Washington, p.802.

Hartmann, P., Leiner, M. J. P. and Lippitsch, M. E. (1995), Response Characteristics of Luminescent Oxygen Sensors, Sensors and Actuators B, 29, 251-257.

Hippensteele, S. A., Russel, L. M. and Stepka, F. S. (1983), Evaluation of a Method for Heat Transfer Measurements and Thermal Visualization Using a Composite of a Heater Element and Liquid Crystals, ASME J. of Heat Transfer 105, 184-189.

Hippensteele, S. A., Russel, L. M. and Torres, F. J. (1985), Local Heat-Transfer Measurements on a Large Scale-Model Turbine Blade Airfoil Using a Composite of a Heater Element and Liquid Crystals, J. Eng. Gas Turbines Power 107, 953-960.

Hubner, J. P., Abbitt, J. D. and Carroll, B. F. (1996), Pressure Measurements on Rotating Machinery Using Lifetime Imaging of Pressure Sensitive Paint, AIAA Paper 96-2934.

Kavandi, J., Callis, J. B., Gouterman, M. P., Khalil, G., Wright, D., Green, E., Burns, D. and McLachlan, B. (1990), Luminescent Barometry in Wind Tunnels, Rev. Sci. Instrum. 61(11), 3340-3347.

Kolodner, P. and Tyson, A. (1982), Microscope Fluorescent Imaging of Surface Temperature Profiles with 0.01 C Resolution, Appl. Phys. Lett. 40(9), 782-784.

Kolodner, P. and Tyson, A. (1983a), Remote Thermal Imaging with 0.7 Micron Spatial Resolution Using Temperature Dependent Fluorescent Thin Films, Appl. Phys. Lett. 42(1), 117-119

Kolodner, P. and Tyson, A. (1983b), Non-contact Surface Temperature Measurement During Reactive-Ion Etching Using Fluorescent Polymer Films, Appl. Phys. Lett. 42(8), 749-751.

Krevelen, D. W. V. (1976), Properties of Polymers, Elsevier, New York.

Lee, Y. and Settles, G. S. (1992), Heat Transfer Measurements and CFD Comparison of Swept Shock/Boundary-Layer Interactions, AIAA Paper 92-3665.

Liu, T., Campbell, T. and Sullivan, J. (1992), Thermal Paints for Shock/Boundary Layer Interaction in Inlet Flows, AIAA Paper 92-3626.

Liu, T., Campbell, B. and Sullivan, J. (1994a), Surface Temperature of a Hot Film on a Wall in Shear Flow, Int. J. Heat Mass Transfer, Vol. 37, No. 17, 2809-2814.

Liu, T., Campbell, B. and Sullivan, J. (1994b), Remote Surface Temperature and Heat Transfer Mapping for a Waverider Model at Mach 10 Using Fluorescent Paint, AIAA Paper 94-2484.

Liu, T., Campbell, B. and Sullivan, J. (1995a), Fluorescent Paint for Measurement of Heat Transfer in Shock-Turbulent Boundary Layer Interaction, Experimental Thermal and Fluid Science 10, 101-112.

Liu, T., Campbell, T., Sullivan, J., Lafferty, J. and Yanta, W. (1995b), Heat Transfer Measurement on a Waverider at Mach 10 Using Fluorescent Paint, J. of Thermophysics and Heat Transfer, Vol. 9, No. 4, 605-611.

Liu, T., Campbell, B. and Sullivan, J. (1995c), Accuracy of Temperature-Sensitive Fluorescent Paint for Heat Transfer Measurements, AIAA Paper 95-2042.

Liu, T. and Sullivan, J. (1996a), Heat Transfer and Flow Structures in an Excited Circular Impinging Jet, Int. J. Heat Mass Transfer, Vol. 39, No. 17, 3695-3706..

Liu, T. (1996b), Applications of Temperature-Sensitive Luminescent Paints in Aerodynamics, Ph.D. Thesis, School of Aeronautics and Astronautics, Purdue University, West Lafayette, IN.

Liu, T., Johnston, R., Torgerson, S., Fleeter, S. and Sullivan, J. (1997), Rotor Blade Pressure Measurement in a High Speed Axial Compressor Using Pressure and Temperature Sensitive Paints, AIAA Paper 97-0162

MacCraith, B. D., McDonagh, C. M., Keeffe, G. O., McEvoy, A. K., Butler, T. and Sheridan, F. R. (1995), Sol-Gel Coatings for Optical Chemical Sensors and Biosensors, Sensors and Actuators B, 29, 51-57.

McLachlan, B. G., Kavandi, J. L., Callis, J. B., Gouterman, M., Green, E. and Khalil, G. (1993a), Surface Pressure Field Mapping Using Luminescent Coatings, Experiments in Fluids 14, 33-41.

McLachlan, B. G., Bell, J. H., Gallery, J., Gouterman, M. and Callis, J. (1993b), Boundary Layer Transition Detection by Luminescence Imaging, AIAA Paper 93-0177.

McLachlan, B. G. and Bell, J. H. (1995a), Pressure-Sensitive Paint in Aerodynamic Testing, Experimental Thermal and Fluid Science, 10, 470-485.

McLachlan, B. G., Bell, J. H., Park, H., Kennelly, R. A., Schreiner, J. A., Smith, S. C., Strong, J. M., Gallery, J. and Gouterman, M. (1995b), Pressure-Sensitive Paint Measurements on Supersonic High-Sweep Oblique Wing Model, Journal of Aircraft, Vol. 32, No. 2, March-April, 217-227.

Meier, B., Werner, T., Klimant, I. and Wolfbeis, O. S. (1995), Novel Oxygen Sensor Material Based on a Ruthenium Bipyridyl Complex Encapsulated in Zeolite Y: Dramatic Differences in the Efficiency of Luminescence Quenching by Oxygen on going from Surface-Adsorbed to Zeolite-Encapsulated Fluorophores, Sensors and Actuators B, 29, 240-245.

Morris, M. J., Benne, M. E., Crites, R. C. and Donovan, J. F. (1993a), Aerodynamics Measurements Based on Photoluminescence, AIAA Paper 93-0175.

Morris, M. J., Donovan, J. F., Kegelman, J. T., Schwab, S. D., Levy, R. L. and Crites, R. C. (1993b), Aerodynamic Applications of Pressure Sensitive Paint, AIAA Journal, Vol. 31, No. 3, March, 419-425.

Morris, M. J. (1995), Use of Pressure-Sensitive Paints in Low-Speed Flows, Proc. 16th Int. Cong. Instrumentation in Aerospace Simulation Facilities (ICIASF), Institute of Electrical and Electronics Engineers, Wright-Patterson Air Force Base, Dayton, OH, USA, 31.1-31.10.

Mulder, M. (1991), Basic Principles of Membrane Technology, Kluwer Academic Publishers, Boston.

Noel, B. W. et al. (1985), A Proposed Method for Remote Thermometry in Turbine Engines, AIAA Paper 85-1468.

Noel, B. W. et al. (1986), Proposed Laser-Induced Fluorescence Method for Remote Thermometry in Turbine Engines, J. Propulsion and Power , Vol. 2, No. 6, 565

Noel, B. W. et al. (1987), Evaluation and Testing Thermographic Phosphors for Turbine-Engine Temperature Measurements, AIAA Paper 87-1761.

Oglesby, D. M., Puram, C. K. and Upchurch, B. T. (1995a), Optimization of Measurements With Pressure Sensitive Paints, NASA TM 4695.

Oglesby, D. M., Leighty, B. D. and Upchurch, B. T. (1995b), Pressure Sensitive Paint With an Internal Reference Luminiphore, Proceedings of the 41st International Instrumentation Symposium, Instrument Society of America, Denver, CO, 381-395.

Oglesby, D. M., Upchurch, B. T., Leighty, B. D. and Simmons, K. A. (1996), Pressure Sensitive Paint With Internal Temperature Sensing Luminiphore, Proceedings of the 42nd International Instrumentation Symposium, Instrument Society of America, San Diego, CA.

Papkovsky, D. B. (1995), New Oxygen Sensors and Their Application to Biosensing, Sensors and Actuators B, 29, 213-218.

Parker, C. A. (1968), Photoluminescence of Solutions, Elsevier Publishing Company, New York.

Peterson, J. I. and Fitzgerald, R. V. (1980), New Technique of Surface Flow Visualization Based on Oxygen Quenching of Fluorescence, Rev. Sci. Instrum. 51(5), 670-671.

Rabek, J. F. (1987), Mechanisms of Photophysical Processes and Photochemical Reactions in Polymer --- Theory and Applications, John Wiley & Sons, New York.

Robinson, P. A. and Perlmutter, D. D. (1994), Oxygen Diffusion and Reaction of Residual Carbon in Sol-Gel-Derived Silica Xerogel, Journal of Non-Crystalline Solids 169, 183-199.

Rodi, P. E. and Dolling, D. S. (1992), Experimental/Computational Studies of Sharp Fin Induced Shock/Turbulent Boundary Layer Interactions at Mach 5: Experimental Results, AIAA Paper 92-0749.

Romano, V., Zweig, A. D., Frenz, M. and Weber, H. P. (1989), Time-Resolved Thermal Microscopy with Fluorescent Films, Appl. Phys. B49, 527-533.

Sacksteder, L., Demas, J. N. and DeGraff, B. A. (1993), Design of Oxygen Sensors Based on Quenching of Luminescent Metal Complexes: Effect of Ligand Size on Heterogeneity, Analytical Chemistry, Vol. 65, No. 23, December 1, 3480-3483.

Sajben, M. (1993), Uncertainty Estimates for Pressure Sensitive Paint Measurements, AIAA J., Vol. 31, No. 11, 2105-2110.

Schultz, D. L. and Jones, T. V. (1973), Heat Transfer Measurements in Short-Duration Hypersonic Facilities, AGARDograph No. 165.

Sellers, M. E. and Brill, J. A. (1994), Demonstration Test of Pressure Sensitive Paint in the AEDC 16-ft Transonic Wind Tunnel Using the TST Model, AIAA Paper 94-2481.

Settles, G. S. and Lu, F. K. (1985), Conical Similarity of Shock/Boundary-Layer Interactions Generated by Swept and Unswept Fins, AIAA J., Vol. 23, No. 7, 1021-1027.

Sholes, R. R. and Small, J. G. (1980), Fluorescent Decay Thermometer with Biological Applications, Rev. Sci. Instrum. 51(7), 882-884.

Song, L. and Fayer, M. D. (1991), Temperature Dependent Intersystem Crossing and Triplet-Triplet Absorption of Rubrene in Solid Solution, Journal of Luminescence 50, 75-81

Sullivan, J. P. (1991), Surface Temperature Measurement Using Fluorescent Molecules, Lecture Notes, Purdue University.

Szmacinski, H. and Lakowicz, J. R. (1995), Fluorescence Lifetime-Based Sensing and Imaging, Sensors and Actuators B, 29, 16-24.

Tobin, K. W., Allison, S. W., Cates, M. R., Capps, G. J., Beshears, D. L., Cyr, M., and Noel, B. W. (1990), High-Temperature Phosphor Thermometry of Rotating Turbine Blades, AIAA J. Vol. 28, No. 8, 1485-1490.

Torgerson, S. D., Liu, T. and Sullivan, J. P. (1996), Use of Pressure Sensitive Paints in Low Speed Flows, AIAA Paper 96-2184.

Torgerson, S. D. (1996), A Laser Scanning System for Use With Pressure and Temperature Sensitive Paints, M. S. Thesis, School of Aeronautics and Astronautics, Purdue University, West Lafayette, IN (to appear).

Troyanovsky, I., Sadovskii, N., Kuzmin, M., Mosharov, V., Orlov, A., Radchenko, V. and Phonov, S. (1993), Set of Luminescence Pressure Sensors for Aerospace Research, Sensors and Actuators B, 11, 201-206.

Uibel, R., Khalil, G., Gouterman, M., Gallery, J. and Callis, J. (1993), Video Luminescent Barometry: The Induction Period, AIAA Paper 93-0179.

Uppal, A. K., Chaturvedi, S. N. and Nath, N. (1987), Temperature-Dependent Photoluminescence & Phosphorescence Decay in CaS:Cu & CaS:Ce Phosphor Using N_2-Pulsed Laser, Indian Journal of Pure & Applied Physics, Vol. 25, Feb. 72-76.

Volan, A. and Alati, L. (1991), A New Optical Pressure Measurement System, Proc. 14th Int. Cong. Instrumentation in Aerospace Simulation Facilities (ICIASF), Institute of Electrical and Electronics Engineers, New York, pp. 10-16.

Wan, J. (1993), Fast Response Luminescent Pressure Sensitive Coating and Derivatives of Tetra (Pentafluorophenyl) Porpholactone, Ph. D Thesis, Department of Chemistry, University of Washington, Seattle, Washington.

Wickersheim, K. and Sun, M. (1985), Phosphors and Fiber Optics Remove Doubt From Difficult Temperature Measurements, Research & Development, November, 114-119.

Winslow, N. A., Carroll, B. F. and Setzer, F. M. (1996), Frequency Response of Pressure Sensitive Paints, AIAA Paper 96-1967.

Xu, W., McDonough, R. C., Langsdorf, B., Demas, J. N. and DeGraff, B. A. (1994), Oxygen Sensors Based on Luminescence Quenching: Interactions of Metal Complexes with the Polymer Supports, Analytical Chemistry, Vol. 66, No. 23, December, 4133-4141.

Table I Temperature-Sensitive Paint Formulations (1)

Paint	λ_{ex} (nm)	λ_{emit} (nm)	Useful temperature sensitive range (^{0}C)	Maximum log slope (%/^{0}C)	Lifetime at room temp.	Reference	Purchase company
Copper complex 2	UV		0 to 80	-0.56		Campbell (1993)	Purdue University
Coumanin in PMMA	UV		20 to 100	-0.4		Campbell (1993)	
CuOEP in GP-197	480-515		-180 to 20	-2.9		Campbell et al. (1994)	
EuTTA in Dope	350	612	-20 to 80	-3.9	1 ms	Liu (1996)	Kodak
EuTTA in PMMA	350	612	-20 to 80	-4.9	330 μs	Campbell (1993)	Kodak
EuTTA in Marathon	350	612	15 to 45 (at least)	-0.95	567 μs	Gallery (1993)	Kodak
Perylene in Dope	330-450	430-580	0 to 100	-1.9	5 ns	Campbell et al. (1994)	Aldrich
Perylenedicarboximide in PMMA	480-515		50 to 100	-0.7		Campbell (1993)	Aldrich
Perylenedicarboximide in Sucrose Octaacetate	480-515		50 to 140	-6		Campbell (1993)	Aldrich
Pyronin B in PMMA	460-580		50 to 100	-4.6		Campbell (1993)	Aldrich
Pyronin Y in Dope	460-580		0 to 100	-5.5		Campbell (1993)	Aldrich
Pyronin Y in PMMA	460-580		60 to 110	-7.2		Campbell (1993)	Aldrich
Pyronin Y in Polycarbonate	460-580		-10 to 100	-3.5		Campbell (1993)	Aldrich
Rhodamine B in Dope	460-590	550-590	0 to 80 (at least)	-1.8		Sullivan (1991)	Aldrich
Rhodamine B in GP-197	460-590	550-590	0 to 50 (at least)	-3.7		Gallery (1993)	Aldrich
Rhodamine B in Polyurethane	UV, 550	618	20 to 175 (at least)	-1.75	4 ns	Romano et al. (1989)	

Note: (1) λ_{ex} and λ_{emit} are the wavelengths of excitation and emission lights, respectively.
(2) Maximum log slope is defined as $\max\{d[\ln(I/I_{ref})]/dT\}$, where I_{ref} is a reference luminescence intensity.
(3) † denotes the thermographic phosphor and ® denotes the proprietary paint.

Table I Temperature-Sensitive Paint Formulations (2)

Paint	λ_{ex} (nm)	λ_{emit} (nm)	Useful temperature sensitive range (^{0}C)	Maximum log slope (%/^{0}C)	Lifetime at room temp.	Reference	Purchase company
Ruthenium (bpy) in GP-197	320, 452	588	5 to 45 (at least)	-2.9		Gallery (1993)	GFS Chemicals
Ruthenium (bpy) in Shellac	320, 452	588	0 to 90 (at least)	-0.93	5 μs	Liu (1996)	GFS Chemicals
Ruthenium (bpy)/Zeolite in Poly Vinyl Alcohol	320, 452	588	-20 to 80	-4.1		Campbell et al. (1994)	GFS Chemicals
Ruthenium (trpy) in Ethanol/Methanol solution	270, 310, 475	620	-180 to -120	-50		Campbell (1993)	Purdue University
Ruthenium (trpy) in GP-197	270, 310, 475	620	-170 to -50	-1.34		Campbell (1993)	Purdue University
Ruthenium (trpy) in Ethyl Cellulose	270, 310, 475	620	-180 to -50	-1.31		Campbell (1993)	Purdue University
Ruthenium (trpy)/Zeolite in Poly Vinyl Alcohol	270, 310, 475	620	-180 to 80	-1.8		Campbell et al. (1994)	Purdue University
Ruthenium complex (VH-127) in GP-197	480-515		-180 to -50	-2.2		Campbell et al. (1994)	Univ. of Houston
Ruthenium complex (SC-324) in GP-197	480-515		-180 to 0	-2.5		Campbell et al. (1994)	Univ. of Houston
Ruthenium complex (VG-225-2) in GP-197	480-515		-180 to 0	-2.2		Campbell et al. (1994)	Univ. of Houston
NASA-Ames and Univ. of Washington TSP ®	UV		0 to 50 (at least)	-3.9		McLachlan et al. (1993b)	Univ. of Washington
McDonnell Douglas TSP ®	340-500	> 500	-5 to 90 (at least)	-2.7		Cattafesta and Moore (1995)	McDonnell Douglas

Table I Temperature-Sensitive Paint Formulations (3)

Paint	λ_{ex} (nm)	λ_{emit} (nm)	Useful temperature sensitive range (^{0}C)	Maximum log slope (%/^{0}C)	Lifetime at room temp.	Reference	Purchase company
CaS:Cu †	337	480	-198 to 2	-0.85	8 μs	Uppal et al. (1987)	
$LaPO_4:Eu^{3+}$ †	280, 395	585, 591	400 to 750	-2.6	3 ms	Bugos (1989)	
La_2O_2S:Eu (537 nm) †	337	537	100 to 200	-3.5	100 μs	Noel et al. (1985)	
La_2O_2S:Eu (514 nm) †	337	514	10 to 90	-3.8	10 μs	Noel et al. (1985)	
$LuPO_4:Eu^{3+}$ †	395	393, 396	700 to 1100	-2.3	3 ms	Bugos (1989)	
Radelin phosphor 1807 †	UV	visible	-20 to 45	-26		Schultz and Jones (1973)	U.S. Radium Corporation
Radelin phosphor 3215 †	UV	visible	0 to 217	-9.2		Schultz and Jones (1973)	U.S. Radium Corporation
Radelin phosphor 2090 †	UV	visible	100 to 317	-5		Schultz and Jones (1973)	U.S. Radium Corporation
Radelin phosphor 3003 †	UV	visible	217 to 427	-5		Schultz and Jones (1973)	U.S. Radium Corporation
$YPO_4:Eu^{3+}$ †	395, 467	593, 618	640 to 1100	-1.8	3 ms	Bugos (1989)	
YVO_4:Eu †	337	618	500 to 725	-2.2	0.5 ms	Tobin et al. (1990)	Martin Marietta, Inc.
Y_2O_3:Eu †	266	611	510 to 1000	-1.88	1.4 ms	Alaruri et al. (1995)	Allison Eng. Company
Y_2O_2S:Tb †	337	545	200 to 550	-2.6	1 ms	Noel et al. (1985)	

Table II Pressure-Sensitive Paint Formulations (1)

Paint	λ_{ex} (nm)	λ_{emit} (nm)	Dynamic range	Stern-Volmer coefficients A_0	A_1	Lifetime at room temp.	Temp. coeff. (%/°C)	Reference	Purchase company
Erythrosin B in silica gel TLC plate	488	575	0.4	0.633	0.367			Burns and Sullivan (1995)	Aldrich
H_2TFPP in silica gel TLC plate	400	654, 702	0.26	0.775	0.225		-0.12	Wan (1993)	Porphyrin Products
H_2TSPP in silica gel TLC plate	400	650, 709	0.44	0.58	0.42			Wan (1993)	Porphyrin Products
$H_2(Me_2N)$TFPP in silica gel TLC plate	400	650	0.56	0.43	0.56		~ 0	Wan (1993)	Produced from H_2TFPP
H_2TCPP in silica gel TLC plate	410	709	0.47	0.4	0.61			Wan (1993)	Porphyrin Products
H_2TNMPP in silica gel TLC plate	420	661, 714	0.57	0.4326	0.5965		~ 0	Wan (1993)	Aldrich
H_2TTMAPP in silica gel TLC plate	410	653, 710	0.62	0.4	0.6			Wan (1993)	Aldrich
PtTFPP in silica gel TLC plate	390	650	0.73	0.27	0.72	50 μs	-2.1	Wan (1993)	Porphyrin Products
PtTFPP in KC18	390	650	0.99	-0.003	0.99	50 μs		Wan (1993)	Porphyrin Products
PtTFPP in Ace white primer	366, 514	650	0.68	0.32	0.68		-1.5	Burns (1995)	Porphyrin Products
PtTFPP in Du Pont Chromaclear	UV, 457-488	650	0.52	0.5	0.52		-1.8		Porphyrin Products

Note: (1) λ_{ex} and λ_{emit} are the wavelengths of excitation and emission lights, respectively.
(2) Dynamic range is defined as $(I_{00} - I_0)/I_{00}$, where I_{00} and I_0 are the luminescence intensities at vacuum and ambient condition, respectively.
(3) Temperature coefficient is defined as $d(I/I_0)/dT$ at ambient conditions.
(4) * denotes the paint that was used as oxygen sensor and ® denotes the proprietary paint.
(5) The Stern-Volmer constants A_0 and A_1 are defined in $I_{ref}/I = A_0 + A_1(P/P_{ref})$, where P_{ref} is the ambient pressure (1 atm).

Table II Pressure-Sensitive Paint Formulations (2)

Paint	λ_{ex} (nm)	λ_{emit} (nm)	Dynamic range	Stern-Volmer coefficients A_0	A_1	Lifetime at room temp.	Temp. coeff. (%/°C)	Reference	Purchase company
PtTFPP in Dope	UV, 457-488	650	0.6	0.43	0.6		-2.3		Porphyrin Products
PtOEP in GP-197	366, 543	650	0.71	0.32	0.7	50 μs	-1.7	McLachlan et al. (1993)	Porphyrin Products
PtOEP in PMMA	366, 543	650	0.386	0.61	0.39	50 μs		Burns and Sullivan (1995)	Porphyrin Products
PtOEP in silica gel TLC plate	366, 543	650	0.88	0.12	0.88	50 μs		Burns and Sullivan (1995)	Porphyrin Products
Perylene dibutyrate (green gold) in silica gel TLC plate	457	520	0.67	0.33	0.67	12.8 ns	4.5	Burns (1995), Wan (1993)	Pylam Products
Perylene dye in silica gel TLC plate	480, 530	550, 570	0.53	0.47	0.53		0.35	Wan (1993)	Aldrich
Pylam yellow in silica gel TLC plate	457	550	0.4	0.59	0.41			Burns (1995)	Pylam Products
Pyrene in silica gel TLC plate	366	490	0.34	0.655	0.345			Burns (1995)	Aldrich
Rose Bengal in silica gel TLC plate	488	590	0.3	0.715	0.285			Burns (1995)	Aldrich
Ru(bpy) in silica gel TLC plate	337, 457	600	0.67	0.33	0.68	3 μs		Burns (1995)	Aldrich
Ru(ph_2-phen) in silica gel TLC plate	337, 457	600	0.82	0.17	0.84	4.7 μs	-1.3	Burns (1995)	GFS Chemicals
Ru(ph_2-phen) in DAP RTV	337, 457	600	0.42	0.58	0.42		-1.2	Burns (1995)	GFS Chemicals
Ru(ph_2-phen) in GE RTV 118	UV, 457	600	0.82	0.27	0.75	1.3 μs	-0.78		GFS Chemicals
bpy/t-Bu in GE RTV 118 *			0.22	0.85	0.16			Sacksteder et al. (1993)	

Table II Pressure-Sensitive Paint Formulations (3)

Paint	λ_{ex} (nm)	λ_{emit} (nm)	Dynamic range	Stern-Volmer coefficients A_0	A_1	Lifetime at room temp.	Temp. coeff. (%/°C)	Reference	Purchase company
Me_4phen/t-Bu in GE RTV 118 *			0.92	0.44	0.55			Sacksteder et al. (1993)	
phen/t-Bu in GE RTV 118 *			0.61	0.65	0.35			Sacksteder et al. (1993)	
$[Ru(ph_2\text{-phen})_3]^{2+}$ in GP-134 mixed with silica *	337	620	0.78	0.217	0.78	0.3 µs		Xu et al. (1994)	
Pd coproporphyrin in PVC + THF membrane *	378, 512, 544	667	0.77	0.227	0.77	200 µs		Gewehr and Delpy (1993)	Porphyrin Products
NASA-Ames PSP1 ®			0.75	0.38	0.62		-1.5	McLachlan and Bell (1995)	NASA Ames
NASA-Ames PSP2 ®			0.65	0.48	0.52			McLachlan and Bell (1995)	NASA Ames
McDonnell Douglas PF2B ®	457	630	0.92	0.084	0.92			Burns (1995)	McDonnell Douglas
McDonnell Douglas PSP 1 ®	488			0.35	0.65			Morris et al. (1993b)	McDonnell Douglas
McDonnell Douglas PSP 2 ®	blue			0.18	0.82			Dowgwillo et al. (1994)	McDonnell Douglas
TsAGI LPSL2 ®	320-350	425-550		0.25	0.75		-0.3	Bukov et al. (1993)	TsAGI
TsAGI LPSF1 ®	320-350	425-550		0.4	0.6		~ 0	Bukov et al. (1993)	TsAGI
TsAGI-INTECO LIPS00R1 ®	visible		0.85	0.2	0.82		-1.1	Troyanovsky et al. (1993)	INTECO and TsAGI
Lumen PSP ®	400-500	550-650	0.86	0.14	0.86		-1	Data sheet by Lumen Corp., Kazakhstan	Global Ventures, US
British Aerospace SRC PSP ®				0.43	0.57		-0.6	Davies et al. (1995)	British Aero. SRC

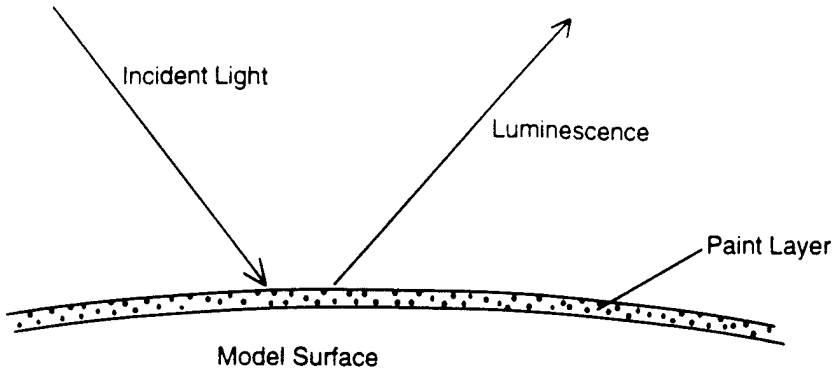

Figure 1 Schematic of a TSP/PSP Layer

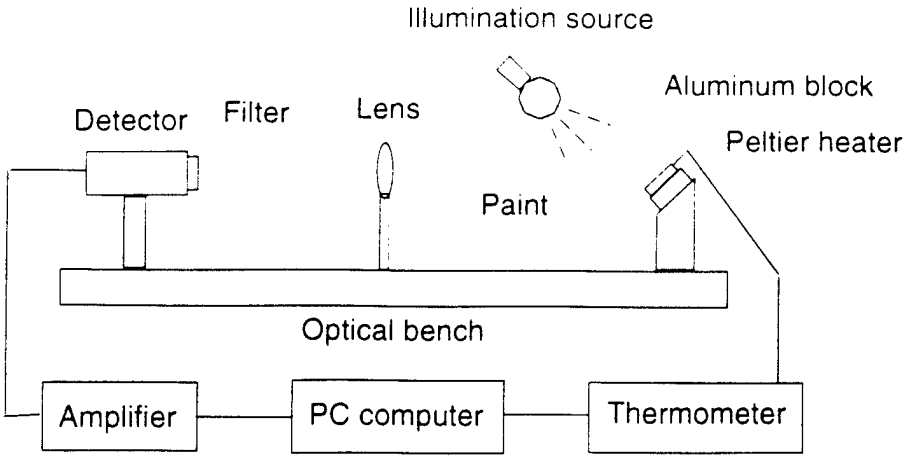

Figure 2 Apparatus for TSP calibration

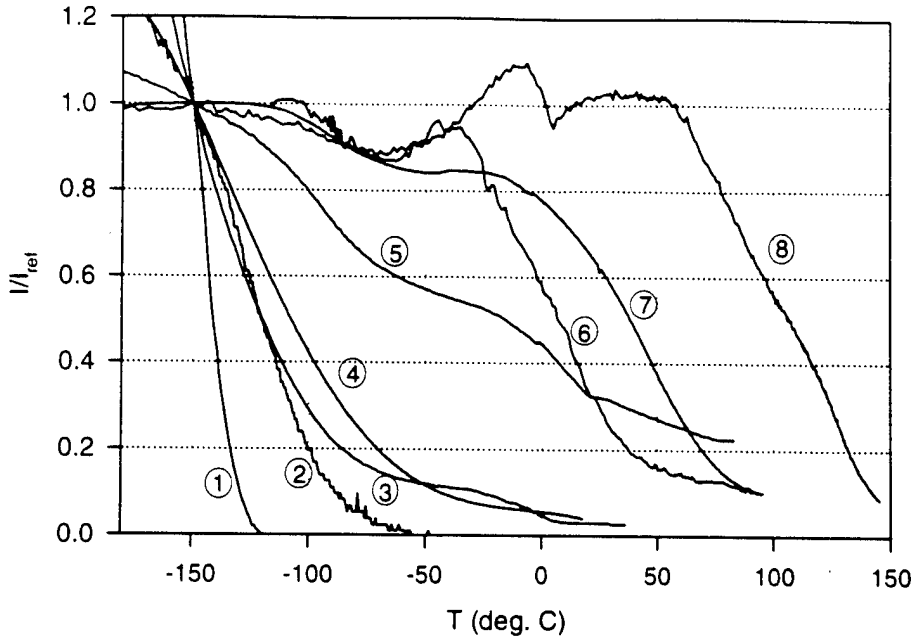

Figure 3 Temperature dependence of luminescence intensity for several TSP formulations: (1) Ru(trpy) in Ethanol/Methanol, (2) Ru(trpy)(phtrpy) in GP-197, (3) Ru(VH127) in GP-197, (4) Ru(trpy) in Du Pont Chroma Clear, (5) Ru(trpy)/Zeolite in GP-197, (6) EuTTA in dope, (7) Ru(bpy) in Du Pont Chroma Clear, (8) Perylenedicarboximide in Sucrose Octaacetate. (T_{ref} = -150 ^{0}C).

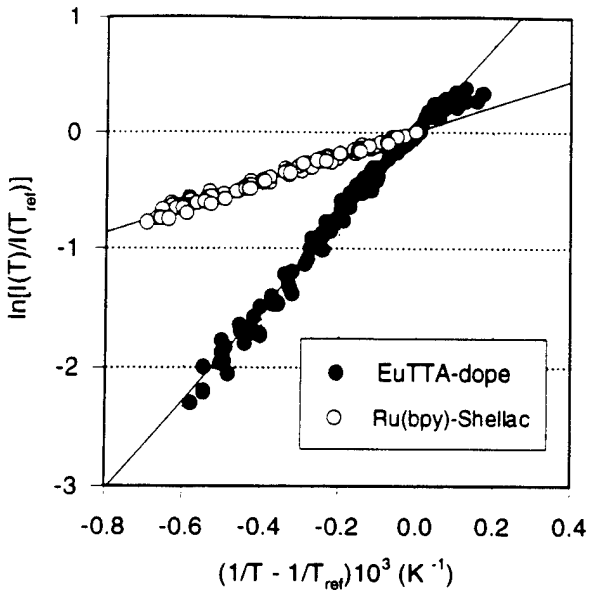

Figure 4 Arrhenius plots for EuTTA-dope and Ru(bpy)-Shellac paints, (T_{ref} = 293 K).

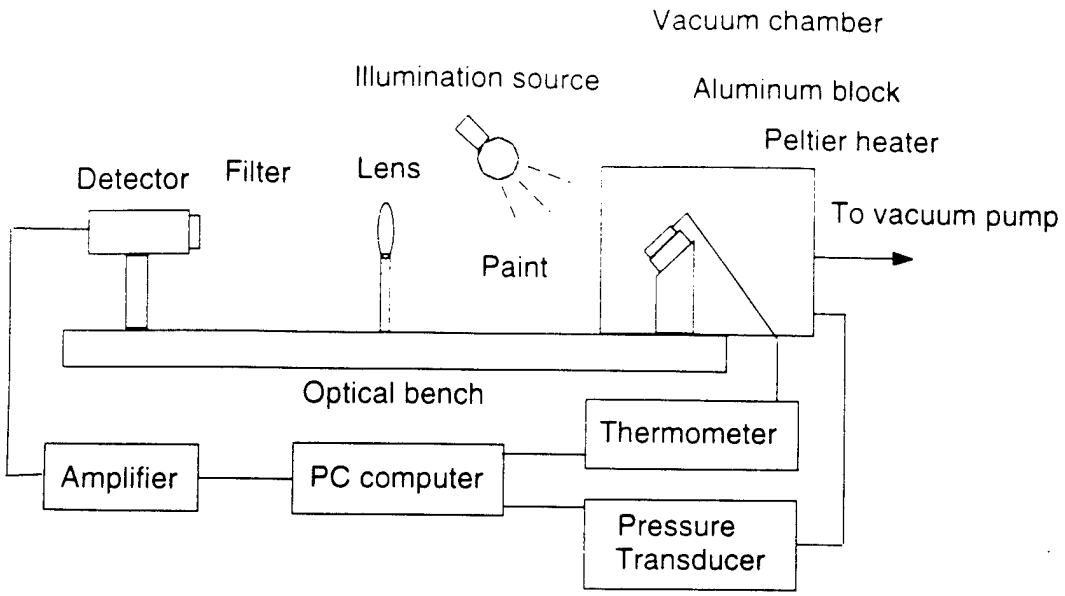

Figure 5 Apparatus for PSP calibration

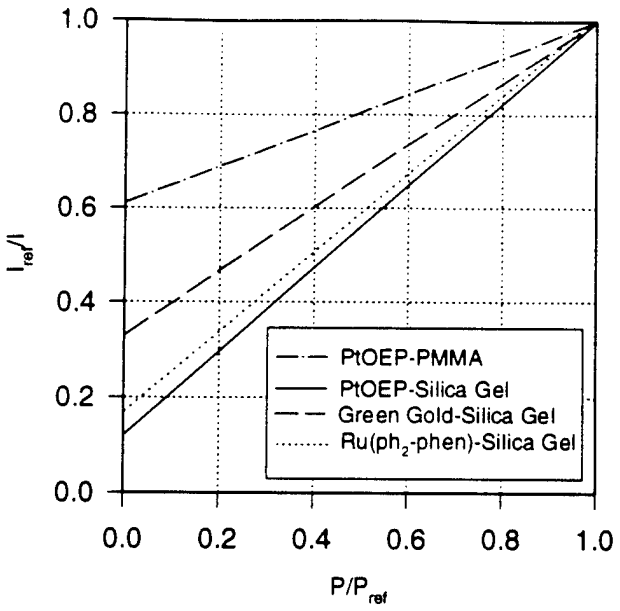

Figure 6 Stern-Volmer plots for several PSPs at ambient temperature (22 ^{0}C), where P_{ref} is the ambient pressure and I_{ref} is the luminescence intensity at ambient conditions. These plots are obtained by fitting experimental data with the Stern-Volmer relation.

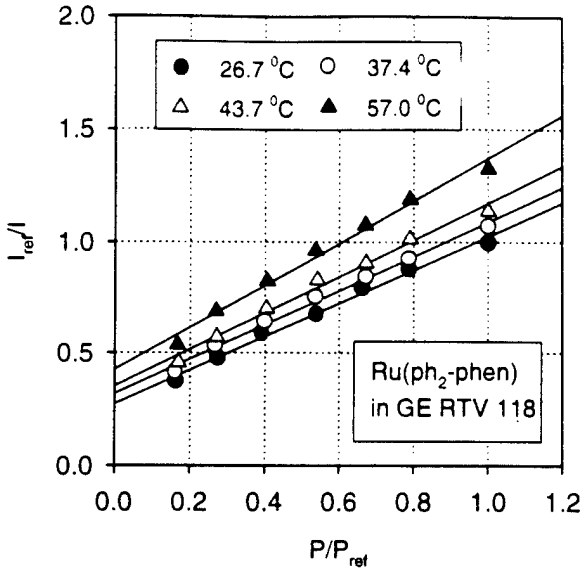

Figure 7 Stern-Volmer plots at different temperatures for Ru(ph$_2$-phen) in GE RTV 118, where P_{ref} is the ambient pressure (1 atm) and I_{ref} is the luminescent intensity at ambient conditions (26.7 ^{0}C and 1 atm).

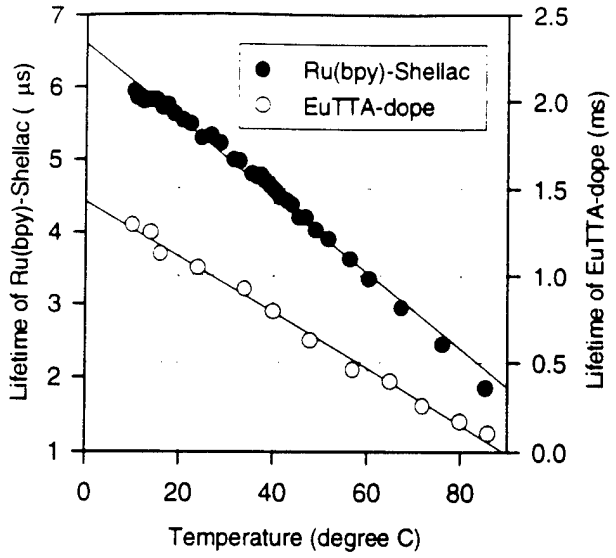

Figure 8 Lifetime-temperature relations for Ru(bpy)-Shellac and EuTTA-dope paints.

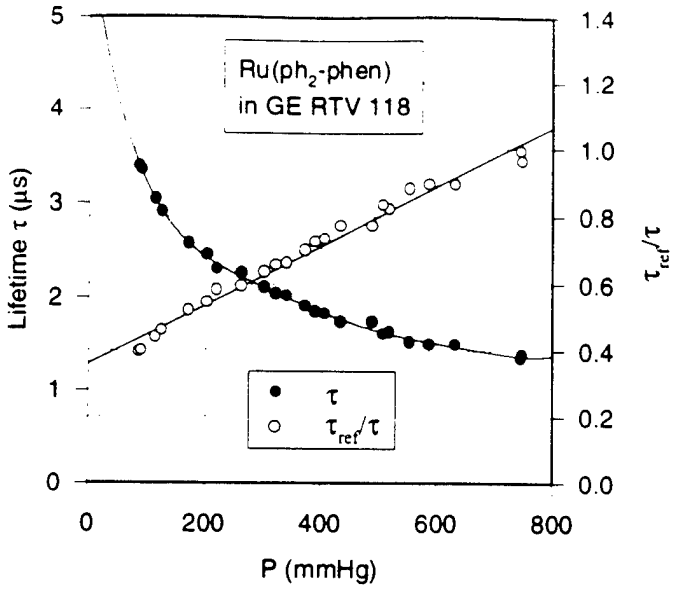

Figure 9 Lifetime-pressure relation for Ru(ph_2-phen) in GE RTV 118 at 22 ^{0}C, where τ_{ref} is the lifetime at ambient pressure.

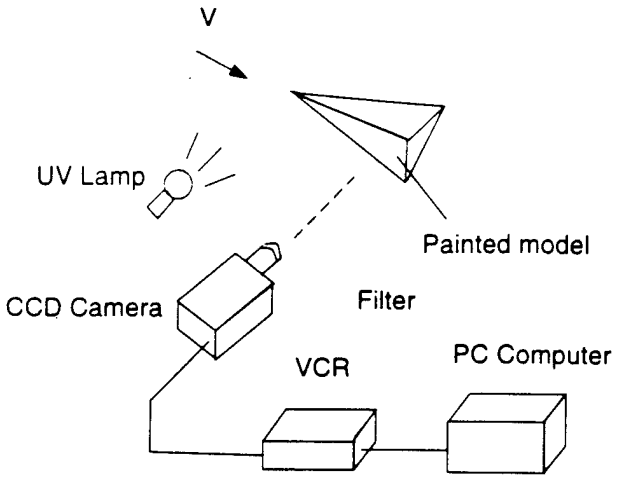

Figure 10 Schematic of CCD camera system

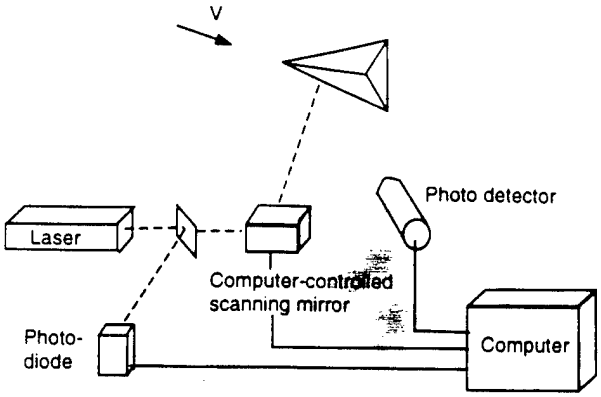

Figure 11 Schematic of laser scanning system

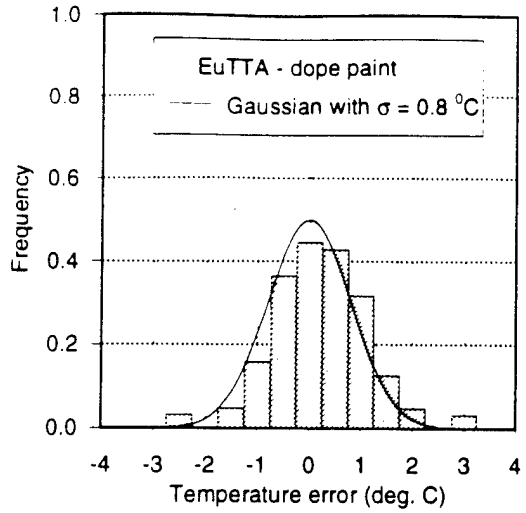

(a)

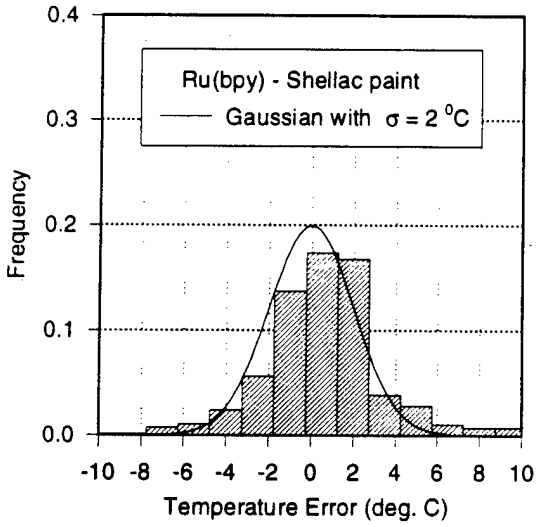

(b)

Figure 12 Temperature calibration error distributions, (a) EuTTA-dope paint, (b) Ru(bpy)-Shellac paint, where σ is the standard deviation.

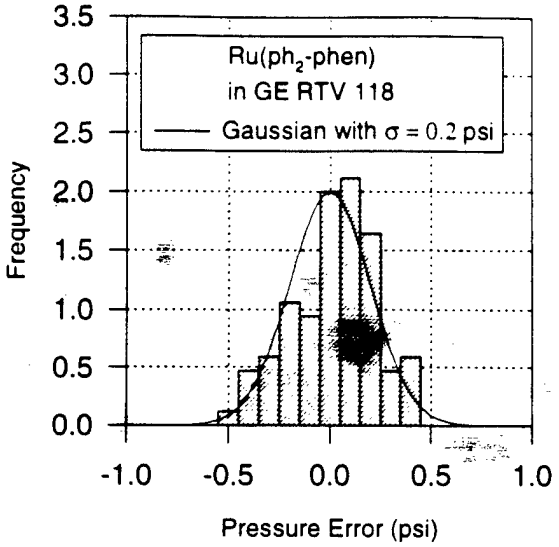

Figure 13 Pressure calibration error distribution for $Ru(ph_2\text{-phen})$ in GE RTV 118, where σ is the standard deviation.

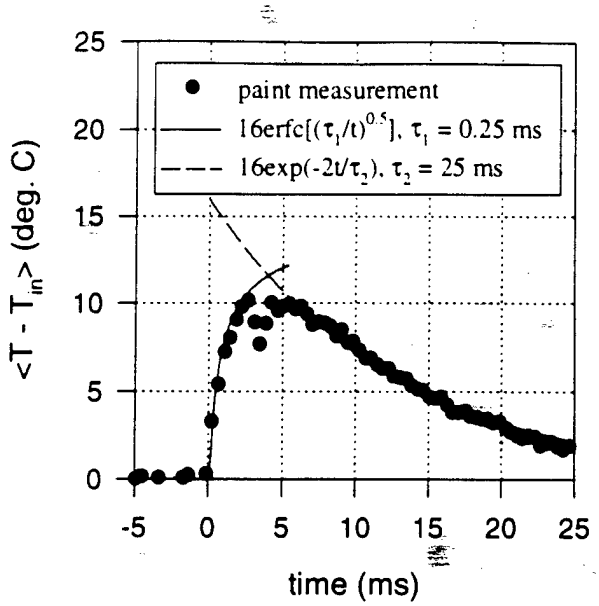

Figure 14 Temperature response of Ru(bpy)-Shellac paint to pulsed laser heating on steel foil.

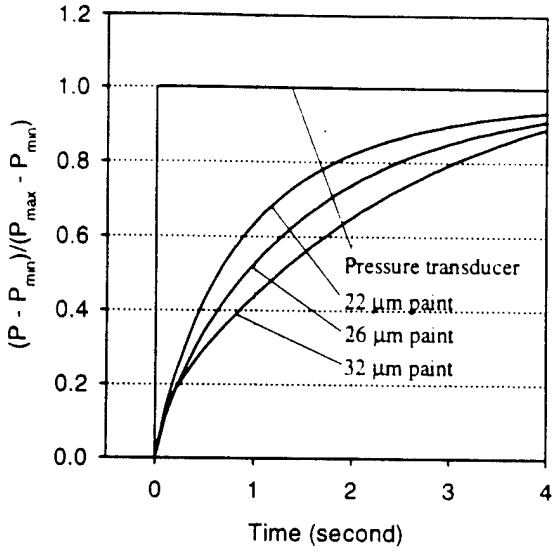

Figure 15 Response of PtOEP in GP-197 to a step change in pressure (from Carroll et al. 1996).

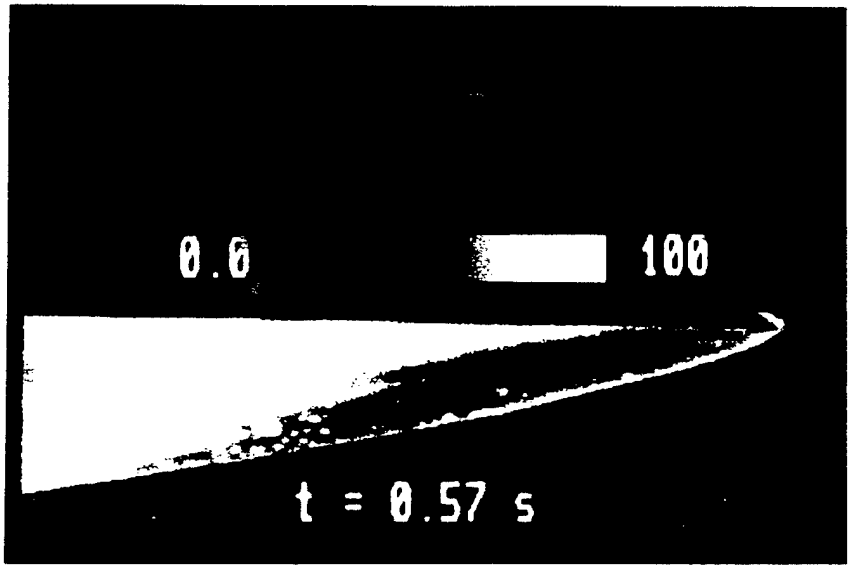

Figure 16 Heat transfer map on the windward side of a Mach 10 waverider model at t = 0.57 s. Flow moves from right to left.

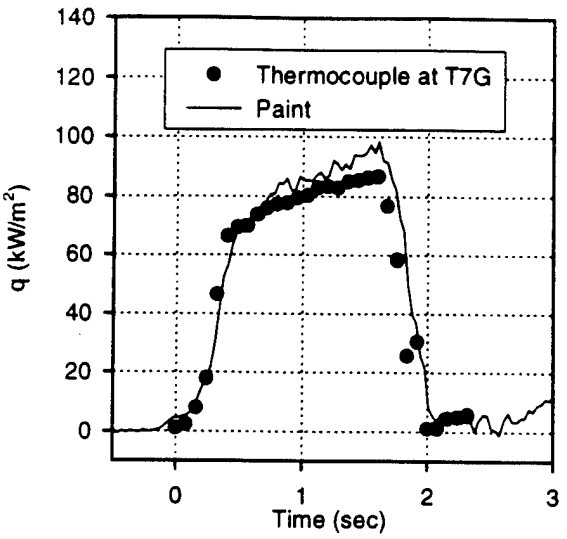

Figure 17 Heat transfer history on a Mach 10 waverider model at location T7G.

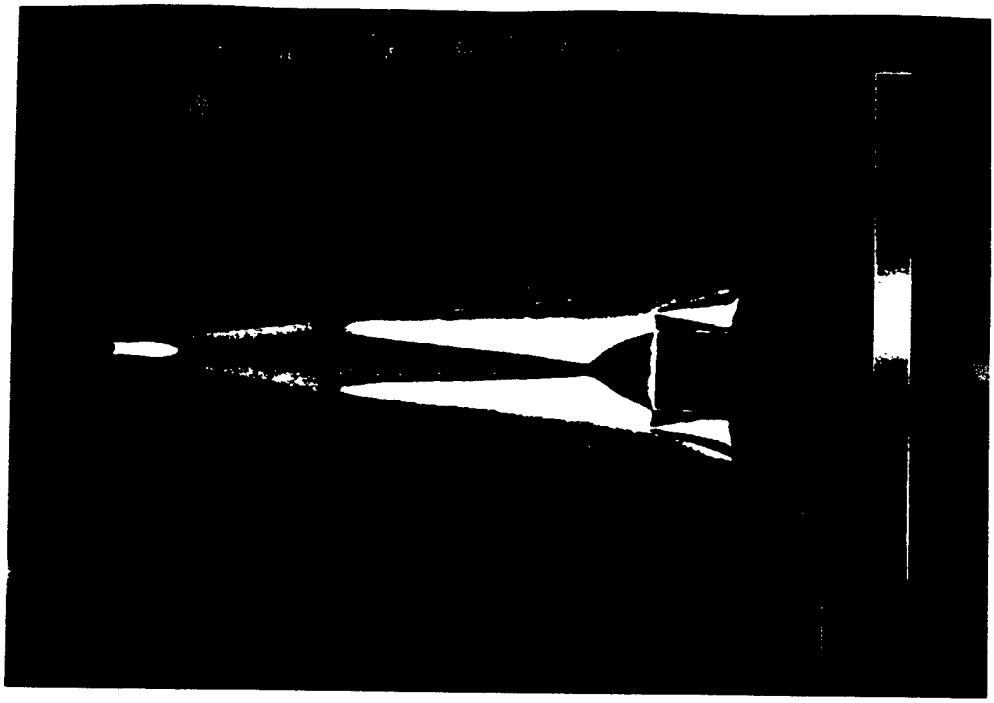

Figure 18 Temperature image on a vertical takeoff/vertical lander concept (from G. Buck and N. R. Merski of NASA-Langley)

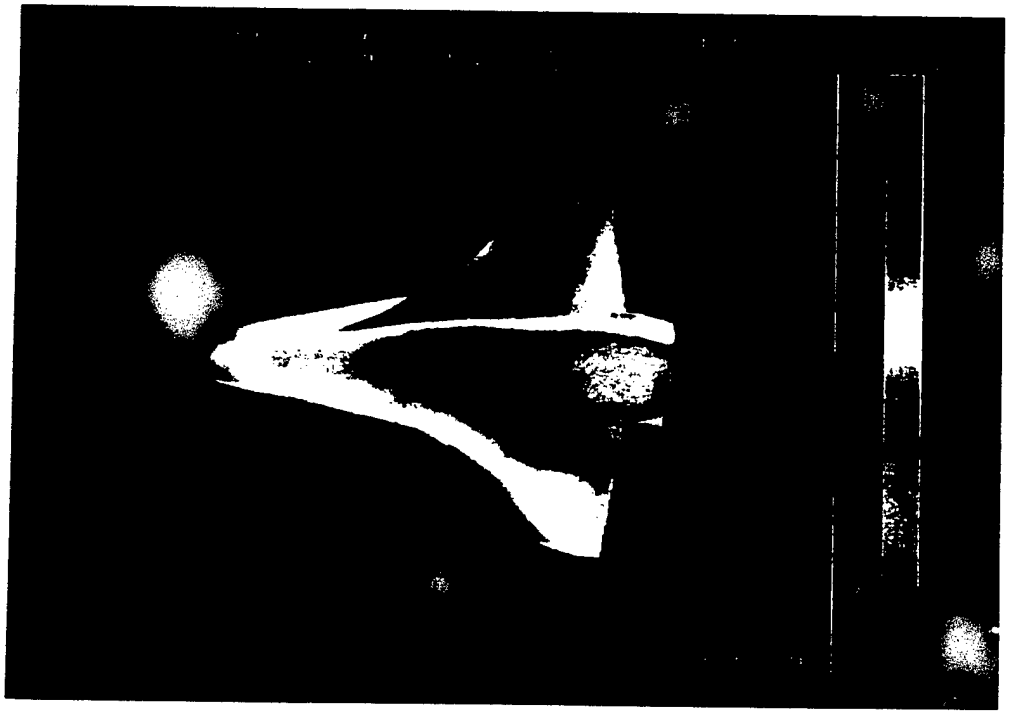

Figure 19 Temperature image on a Shuttle Orbiter model (from G. Buck, S. A. Berry and G. Brauckmann of NASA-Langley)

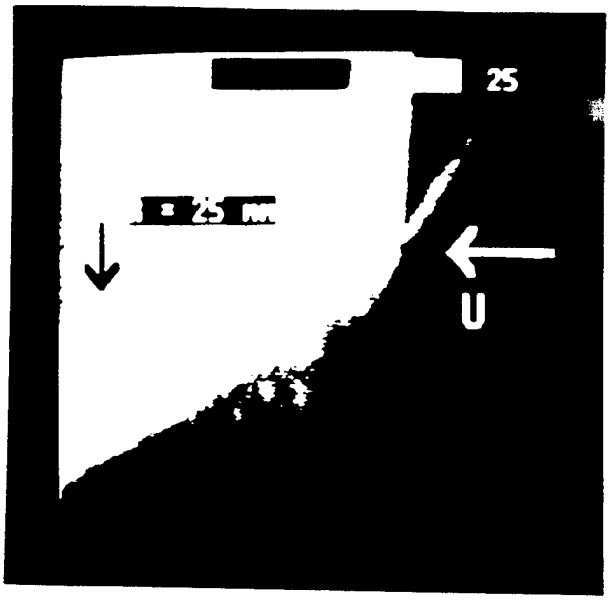

Figure 20 Heat transfer map in swept shock/boundary layer interaction at Mach 2.5.

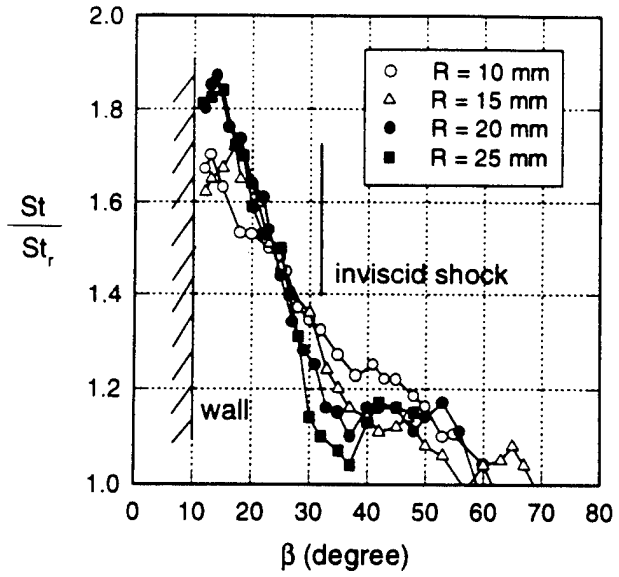

Figure 21 Relative Stanton number distributions at four radial distances in swept shock/boundary layer interaction at Mach 2.5.

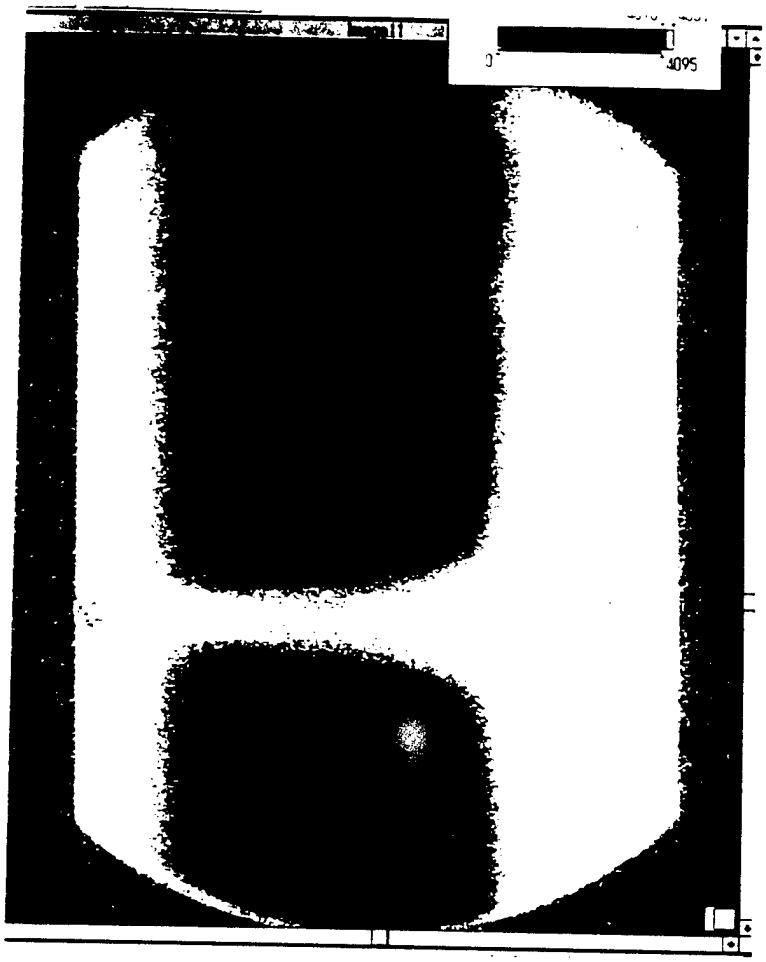

Figure 22 Transition image on a NACA 64A012 airfoil in a cryogenic wind tunnel where total temperature is 150 K and Mach number is 0.4. Flow moves from left to right.

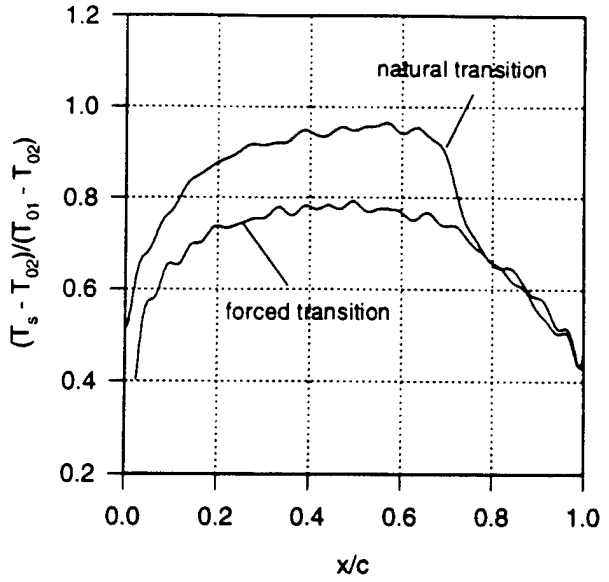

Figure 23 Chordwise surface temperature distributions in natural and forced transition regions on a NACA 64A012 airfoil in a cryogenic wind tunnel (T_{01} = 150 K and T_{02} = 142.5 K)

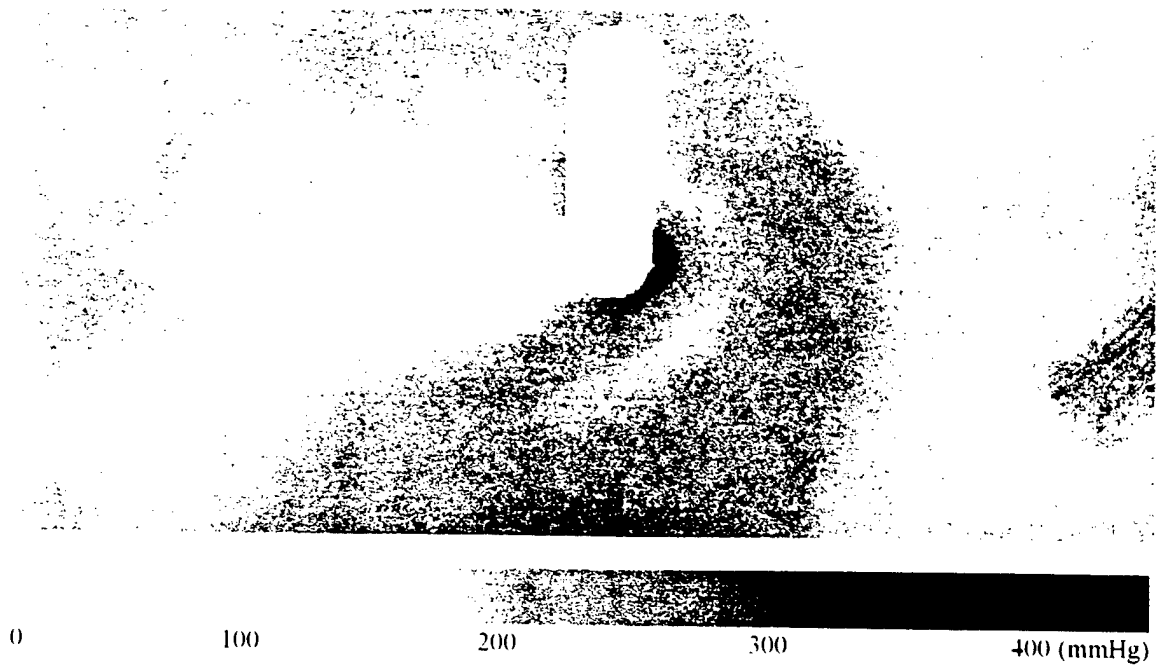

Figure 24 Surface pressure map for the interaction of a cylinder with a supersonic turbulent boundary layer at Mach 2.5. Flow moves from right to left.

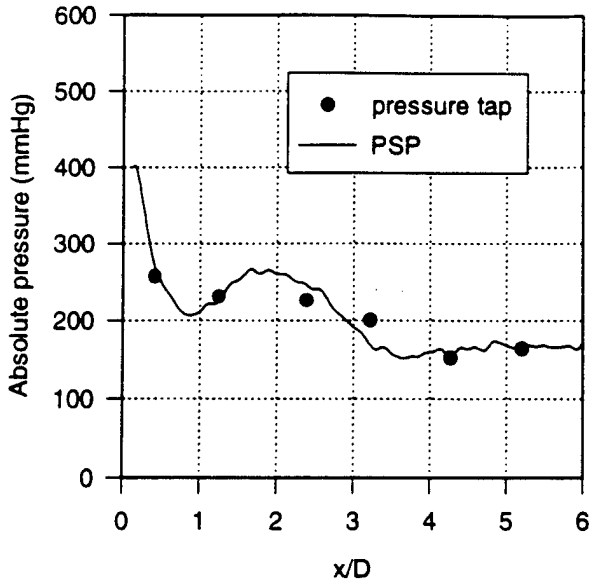

Figure 25 Centerline pressure distribution for the interaction of a cylinder with a supersonic turbulent boundary layer at Mach 2.5.

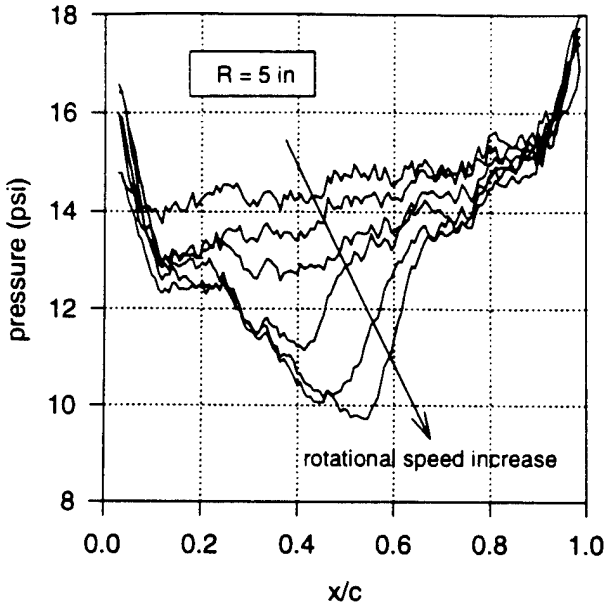

Figure 26 PSP pressure distributions on the suction surface of a compressor rotor blade at a radius of 5 inches (mid-span) for different rotational speeds (10000, 13500, 14750, 16000, 17000, and 17800 rpm).